

# Translational Dynamics of Rod-like Particles in Supercooled Liquids : Probing Dynamic Heterogeneity and Amorphous Order

Anoop Mutneja\* and Smarajit Karmakar†

Tata Institute of Fundamental Research, 36/P,Gopanpally Village,  
Serilingampally Mandal,Ranga Reddy District, Hyderabad, 500107, India

(Dated: March 30, 2021)

The use of probe molecules to extract the local dynamical and structural properties of complex dynamical systems is an age-old technique both in simulations and experiments. A lot of important information which is not immediately accessible from the bulk measurements can be accessed via these local measurements. Still, a detailed understanding of how a probe particle's dynamics are affected by the surrounding liquid medium is not very well understood, especially in the supercooled temperature regime. This work shows how translational dynamics of a rod-like particle immersed in a supercooled liquid can give us information on the growth of the correlation length scale associated with dynamical heterogeneity and the multi-body static correlations in the medium. A unified scaling theory rationalizes all the observed results leading to the development of a novel yet simple method that is accessible in experiments to measure the growth of these important length-scales in molecular glass-forming liquids.

*Introduction:* Supercooled liquids are structurally almost indistinguishable from their high-temperature liquid state structures as probed using various scattering experiments. Even with a significant decrease in temperature, they remain so unlike the normal crystallization phenomenon where continuous translational symmetry is broken and crystalline order sets in at freezing transition leading to the appearance of rigidity. The similar appearance of rigidity in supercooled liquids while approaching the so-called calorimetric glass transition temperature manifests itself in the massive increase in the viscosity (or structural relaxation time) of the system [1] with no emerging apparent structural order, which makes it extremely hard to rationalize [2]. But on the other hand, the individual particles of supercooled liquids are found to be dynamically correlated to each other over a length scale of  $\xi_d(T)$  that grows with increasing supercooling [2–5]. This knowledge portrays a picture of the supercooled liquid state as a medium of different spatial regions with very different dynamical properties, often given the name of Dynamical Heterogeneity (DH) in the literature[3–6]. The framework of DH can very efficiently explain the experimentally observed features like stretched exponential relaxation, decoupling of viscosity and diffusion constant, non-Gaussian self part of van Hove function, rotation-translation decoupling [3, 7, 8], etc. Previous experiments on colloidal glasses also confirm the growth of  $\xi_d(T)$  [9–11]. However, its experimental measurements in molecular liquids like glycerol, *ortho*-terphenyl (OTP), sorbitol, etc., remain a challenge. Only a handful of complicated procedures exist if one wants to measure the same in experiments using higher order correlation functions[12].

On the other hand, as suggested in previous works [4, 13, 14], the growing, dynamical correlations seem to not causally account for the rapid growth of liquid's viscosity or structural relaxation time. There has to be an accompanying increase of some static correlation often termed in the literature as "Amorphous order" [15, 16]. This growth of correlation amongst disorder manifests itself in the observed finite-size effects of the lowest vibrational frequency of the dynamical (Hessian) ma-

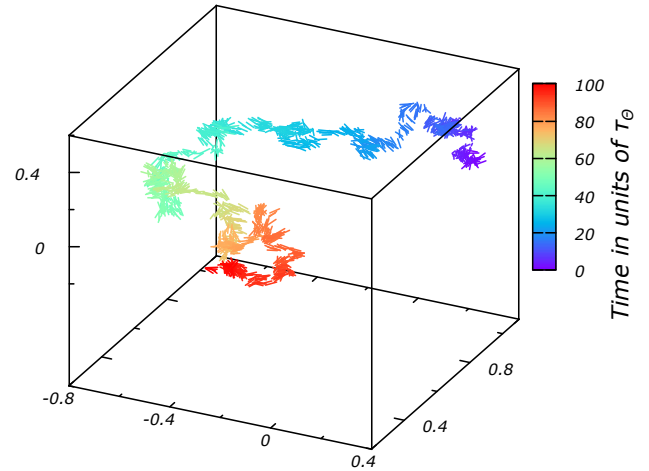


FIG. 1. The rod's trajectory in a model supercooled liquid at low temperature. The color bar represents the rod's time evolution in the units if  $\tau_\theta$ , where  $\tau_\theta$  is the averaged time taken for a rod to rotate by unit radian. A cage motion with intermittent jumps clearly signifies the underlying heterogeneity in the embedding supercooled liquid medium's dynamics.

trix [17], of structural relaxation time  $\tau_\alpha$  (defined later) [13], etc. Thus, this correlation can be measured via careful finite-size scaling (FSS) of these quantities [4, 13, 17]. This length scale is also related to configurational entropy  $S_c$  proposed in Adam-Gibbs relation [15], hence giving other ways to quantify it in the simulations [13]. Alternatively, this static correlation can also be measured using the so-called point-to-set (PTS) correlation function [18]. Still, this method will apply only to simulations and colloidal experiments due to its complex procedure. On the other hand, for molecular liquids, the existing experimental measurements for growing static correlation are extremely subtle and are done by measuring the fifth-order dielectric susceptibility  $\chi_5(t)$  in supercooled glycerol and propylene [19]. Thus it won't be incorrect to say that

the present-day experiments are not equipped to quantify both static and dynamic length scale in molecular supercooled liquids easily. Any new proposal for the experimental method to quantify both these length-scales would then be highly welcomed. Future insights in growth of these two length scales would have far-reaching implications in developing a unified theory of glass transition and industrial applications like bio-preservation [20–24].

The new method proposed in this letter can also lead to a better understanding of the existing results of single-molecule (SM) experiments and, at the same time, help us simultaneously extract the important length scales of the system. In the current SM experimental results, the dynamical heterogeneity is quantified either via decoupling of rotational and translational motions of probe molecules or by the observed broadening in the rotational relaxation time distribution,  $\tau_\theta$  (see SI for definition) [3, 7, 8, 25]. The observed decoupling between rotational and translational motions of elongated probe molecules can be very well rationalized by dynamical heterogeneity in the medium. On the other hand, the observed broadening in the rotation relaxation time, although claimed to be a direct implication of dynamical heterogeneity, is related to the growing static length scale of amorphous order. In a recent work [26], the exact form of the distribution of rotational relaxation time has been derived in the high-temperature limit, and deviation from this asymptotic form is then used to quantitatively measure the growth of static length scale via an elegant scaling analysis. Similarly, dynamic length scale  $\xi_D$  is shown to be obtained from the scaling analysis of the non-normal parameter [27], which measures the deviation in rotational displacement distribution from the usual high-temperature homogeneous behaviour. In this letter, we have done a detailed study of the dynamical effects induced by the supercooled liquid environment on the translational dynamics of the center of mass (CoM) of a probe particle with an increasing degree of supercooling and for different probe sizes.

The main idea behind this work is as follows, on spatial coarse-graining of the supercooled medium over a length scale similar or larger than the underlying correlation length, the system will start to behave like a homogeneous liquid medium [26, 28, 29]. This coarse-graining procedure unfortunately would require one to have the positions of all the constituent particles in the system across various timescales, but this will be nearly impossible to implement for molecular liquids. One can avoid this difficulty by obtaining the system's response averaged over the desired length scale via a probe molecule. This is precisely the idea used in this work to extract the liquid medium's response at various length scales by systematically changing the probe size similar to the SM experiments. The SM probes of different linear lengths would effectively probe the system at the respective coarse-graining length and significantly reduce the experimental complexity. The only task at hand would be to appropriately choose the probes of various sizes for a given supercooled liquid and study their dynamics as a function of the varying probe length. In Ref.[26], the va-

lidity of this concept has been rigorously established for the rod's rotational dynamics (probe) molecule. In this letter, we show how dynamical and structural information can be obtained similarly using the translational motion of the CoM of a rod with the possibility of lesser experimental complexity.

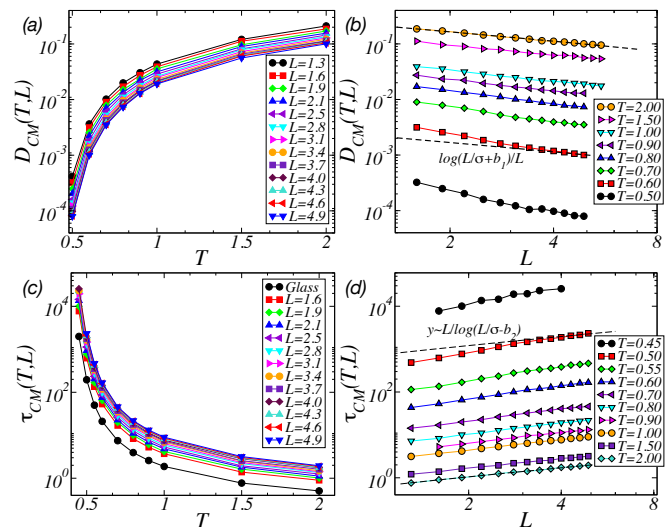


FIG. 2. Left Panels: Temperature variation of the diffusion constant,  $D_{CM}$  (top) and the relaxation time,  $\tau_{CM}$  (bottom) of CoM of the rod of different lengths immersed in 3dKA medium. Right Panels: Rod-length variation of  $D_{CM}$  and  $\tau_{CM}$  for rods immersed in 3dKA system at different temperatures. The rod-length variation for small rod lengths and high-temperature regimes matches the Brownian particle's predicted hydrodynamic expression (dotted lines).

**Models and Methods:** This work contains extensive simulations of two model glass-forming liquids, namely - (i) the Kob-Andersen 80 : 20 binary Lennard-Jones mixture (3dKA) [30] and (ii) the 50 : 50 binary mixture of particles interacting via harmonic potential (3dHP) [31] in three dimensions. We have not looked at models in two dimensions primarily because of long-wavelength fluctuations arising due to the Mermin-Wagner theorem, which affects quantities related to particles' translational motion in two dimensions [32, 33]. Although these effects can be taken care of systematically by computing appropriate correlation functions [33–36], thus the results presented in this paper are not limited to three-dimensional systems only. The units of length, energy, and time are the diameter of the larger particle ( $\sigma$ ), the pre-factor of the potential energy function ( $\epsilon$ ), and  $(\sqrt{m\sigma^2/\epsilon})$ , respectively. Here  $m$  is the mass of a constituent particle. The other reduced units can be derived from these units. Further details of the models, and the techniques used to perform the constant number of particle ( $N$ ), pressure ( $P$ ) and temperature  $T$  molecular dynamics simulations (NPT) with few rod-like particles are given in the SI. We want to highlight that we have chosen these two model systems in this study primarily to understand the generic nature of the presented results. The 3dKA model is developed to model the supercooled liquid dynamics of molecular glass-forming liquids. The 3dHP

model is a paradigmatic model to study jamming physics in the context of dense, soft sphere systems and soft granular particles, including colloidal particles in experiments. The rest of the letter is broadly divided into two parts. In the first part, we discuss the scaling analysis performed to extract the static length scale,  $\xi_S$ , from the rod length dependence of relaxation time and diffusion coefficient. Then, we discuss the Stokes-Einstein (SE) and Stokes-Einstein-Debye (SED) relation in the same context and show how the departure from both SE and SED relation can be used to obtain the growth of the underlying dynamic length scale,  $\xi_D$ . It is fascinating to see how all the probe particle's dynamical behaviour can be rationalized using these two length scales in the system via an elegant scaling analysis.

*Translational diffusion constant  $D_{CM}(T, L)$  & relaxation time  $\tau_{CM}(T, L)$ :* The essential quantities to study for translational dynamics of rods would be the mean squared displacement (MSD) and the two-point overlap correlation function ( $Q(t)$ ) of the CoM of the rods. Also, since the rotational correlations for large enough rods can survive for substantially long times in supercooled liquids, the MSD of the rod along its initial orientation and perpendicular to it would provide us insight into the translational anisotropy of probe rods. Further detailed characterizations, including the definitions of MSD and  $Q(t)$ , are given in the SI. The diffusion constant  $D_{CM}(T, L)$  and the relaxation time  $\tau_{CM}(T, L)$  of the CoM motion of the rod can be estimated from MSD and  $Q(t)$ , respectively (see SI for details). The temperature dependence of  $D_{CM}$  and  $\tau_{CM}$  for different rod lengths and the rod length dependence at different supercooling temperatures for the 3dKA model are shown in Fig.2. Also, the plots are similar for the 3dHP model and can be found in SI. In a homogeneous liquid, the diffusion constant of a Brownian rod should decrease with rod length as  $D_{CM} \sim \ln(L/\sigma + b_1)/L$ , if one considers the hydrodynamic interaction with the surrounding medium. Here  $\sigma$  is the rod's width, and  $b_1$  is a correction factor arising due to the drag effect coming from the two ends of the rod (see Ref.[37] for details). Similarly, relaxation time will increase as  $\tau_{CM} \sim L/\ln(L/\sigma + b_2)$  in the large rod and high-temperature limit with a different constant,  $b_2$ . This dependence can be clearly seen in the right panels of Fig.2. Thus,  $\ln(L)/L$  like dependence in  $D_{CM}$  can be attributed solely to the rod's translational properties in a homogeneous liquid medium. Any subsequent deviation from this behaviour at either smaller rod length or lower temperature can be thought of as the effect of growing correlations in the medium due to supercooling.

Interestingly, both of these quantities start to show violation from logarithmic dependence below a critical rod length that increases with increasing supercooling. Physically, both of these violations imply the faster translational diffusion of smaller rods in a supercooled environment than it should have been according to the underlying homogeneous liquid behaviour. This behaviour is very similar to the observed rotational hops in the previous work [26], making the smaller probes rotationally decorrelate at a shorter time than expected.

This anomaly was linked with the underlying growing static correlations, so we can expect that the growth of the same static length scale can be the cause here. The measured increase (decrease) in  $D_{CM}(T, L)$  ( $\tau_{CM}(T, L)$ ) should then be an effect of this emerging structural order.

To extract the underlying length scale, we first scale-out the asymptotic high-temperature and large rod length dependence and look at the parameter  $\tilde{D}(T, L) = D_{CM}L/\ln(L/\sigma + b_1)$ .  $\tilde{D}$  is then scaled by its large rod-length value at each temperature  $T$ , i.e.,  $\tilde{D}^*(T) = \tilde{D}(T, L \rightarrow \infty)$ . In the top left panel of Fig.3 we show  $\tilde{D}(T, L)/\tilde{D}^*(T)$  as a function of rod length  $L$ . It is clear that deviation from high temperature large rod-limit asymptote becomes prominent with decreasing temperature, suggesting growth of underlying correlation length in the system. Data for all temperature and rod lengths can then be collapsed by plotting  $\tilde{D}(T, L)/\tilde{D}^*(T)$  as a function of  $L/\xi_{CM}^D$ , where  $\xi_{CM}^D$  is the underlying length scale if one assumes the following scaling ansatz.

$$\frac{\tilde{D}(T, L)}{\tilde{D}^*(T)} = \mathcal{F}(L/\xi_{CM}^D). \quad (1)$$

A good data collapse in the middle panel of Fig.3 clearly demonstrates the validity of the scaling assumptions. Similarly, the length scale  $\xi_{CM}^\tau$  can be obtained from the relaxation time (See top right panel of Fig.3), if we assume a similar scaling ansatz as

$$\frac{\tilde{\tau}(T, L)}{\tilde{\tau}^*(T)} = \mathcal{G}(L/\xi_{CM}^\tau), \quad (2)$$

where  $\tilde{\tau}(T, L) = \tau_{CM} \ln(L/\sigma + b_2)/L$  and  $\tilde{\tau}^*(T) = \tilde{\tau}(T, L \rightarrow \infty)$ . The comparison of obtained length scale with the static length scale of liquid is presented in the respective insets. The similarity observed in their temperature dependence establishes the robustness of the method. A similar analysis for the 3dHP model as shown in the bottom panels of the same figure suggests the method's generic nature across various model systems that are very different. Surprisingly, the scaling functions used for the  $D_{CM}$  and  $\tau_{CM}$  scaling analysis (see Eqs. 1 and 2) turn out to be inverse of each other, leading to a strong coupling between them. Thus if one plots  $\tilde{D}_{CM}$  as a function of  $\tilde{\tau}_{CM}$ , then one observes fantastic data collapse for all temperatures and rod lengths as shown in the top left panel of Fig.4. The lovely master curve implies that even in low temperatures,  $\tilde{D}_{CM}$  and  $\tilde{\tau}_{CM}$  obey the Stokes-Einstein (SE) relation  $\tilde{D}_{CM}(L, T)\tilde{\tau}_{CM}(L, T) = \text{constant}$  as will be discussed in the subsequent paragraphs.

*Stokes-Einstein Breakdown (SEB):* Stokes-Einstein (SE) relation is the blend of Einstein's equation for diffusion constant and Stokes's equation for drag coefficient for a spherical particle in a homogeneous medium. It reads as  $D = k_B T/c\pi R\eta$ , where  $D$  and  $R$  respectively are the diffusion constant and the particle's hydrodynamic radius.  $\eta$  and  $T$  are the shear viscosity and the liquid's temperature, respectively, and  $c$  is a constant which depends on the boundary condition at the particle's surface ( $c = 6$  for stick &  $c = 4$  for slip) [38].

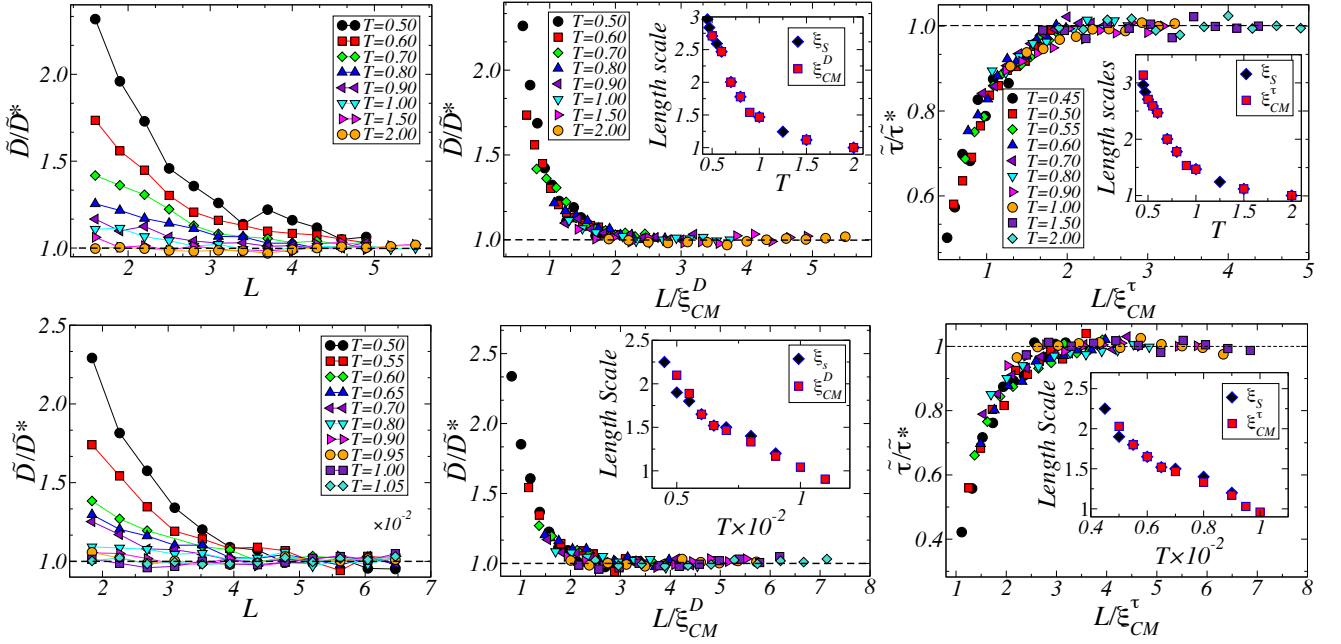


FIG. 3. Top-Panel: In the left-panel,  $\tilde{D}/\tilde{D}^*$  is plotted against the rod length of rods in different supercooling temperatures of the 3dKA model. Here  $\tilde{D}(T, L)$  is the  $D_{CM}$  with the rod-length dependence of homogeneous medium removed and  $\tilde{D}^*(T) = \tilde{D}(T, L \rightarrow \infty)$ . The parameter  $\tilde{D}/\tilde{D}^*$  deviates from the homogeneous behaviour (constant in  $L$ ) at larger and larger rod lengths with increasing supercooling (while approaching from large rod-length). Center-panel contains the data collapse of  $\tilde{D}/\tilde{D}^*$  using the scaling ansatz of Eq.1. The temperature dependence of the obtained length scale is similar to that of the system's static length scale computed using the PTS method (center-inset) [28]. Right-panel shows the similar data collapse for  $\tilde{\tau}/\tilde{\tau}^*(T)$  using Eq.2 and compares the obtained length scale to the PTS static length scale [28] in the inset. The bottom-panels have similar plots for the 3dHP model.

$k_B$  is the Boltzmann constant. This expression is also valid for the self-diffusion of the liquid particles. Breakdown of this famous Stokes-Einstein relation is believed to be one of the hallmarks of dynamic heterogeneity in supercooled glass-forming liquids. Since the distribution of local viscosity or structural relaxation time gets broader due to dynamic heterogeneity, the diffusion constant's growth becomes faster than the predicted value from SE relation. The viscosity in this expression is often replaced by  $\tau \sim \eta/T$ , as the growth of these two quantities is essentially the same over the studied temperature range. Thus the Stokes-Einstein relation for a rod-like particle will read as,

$$D\tau = \frac{1}{c\pi R} = f(R). \quad (3)$$

$f(R)$  can be considered as a measure of SEB. Now, for dynamics of rods in the liquid, one can have  $D_{CM}\tau_{CM}$  as well as  $D_{CM}\tau_\alpha$  as possible SEB parameters. Where  $D_{CM}$  &  $\tau_{CM}$  are the diffusion constant and relaxation time of CoM of the rod and  $\tau_\alpha$  is the relaxation time of liquid (see SI for definition). These two SEB parameters look at the validity of SE relation for the rod's self dynamics and the coupling of the dynamics of the rod with the liquid medium. Thus, it gives rise to a possibility of understanding how dynamical information of liquid can be obtained from the rod's dynamics in that medium. The top-left panel of Fig.4 confirms the validity of the SE relation for  $D_{CM}$  and  $\tau_{CM}$  of the rod particles. This

tells us that the SE relation between the rod's diffusion constant and relaxation time is obeyed for all temperatures, even deep in the supercooled liquid regime for all rod lengths.

Surprisingly, the fractional SE relation  $D_{CM} \sim \tau_\alpha^{-\omega}$  seems to be obeyed in the large-rod-length and high-temperature limit with an emerging power-law exponent  $\omega = 1.25$ . Note that exponent is bigger than 1, and in supercooled liquids, with diffusion constant and relaxation time of the liquid, one sees similar power-law dependence with exponent  $\omega$  smaller than 1. Although we do not have a microscopic understanding of this exponent's value for rod-like particles, it is interesting to note that this exponent seems universal across the two model systems that we have looked at in this work. Note that for smaller rod lengths, the power-law dependence appears to be deviating from the asymptotic behaviour, which can be quantified if we plot  $D_{CM}\tau_\alpha^\omega$  as a function of inverse temperature as shown in Fig.4 (bottom-left) for different rods. As seen, this parameter remains almost constant for the largest rod for the entire temperature range, with deviation showing up at the lowest studied temperature. The SE breakdown starts to happen at a higher and higher temperature with decreasing rod length, as shown in the top right panel of Fig.4. This behaviour is remarkably similar to the results reported in Ref. [39] for the wave vector ( $k$ ) dependence of SEB. It was found that the SEB at various  $k$  occurs at lower and lower temperatures as one decreases the value



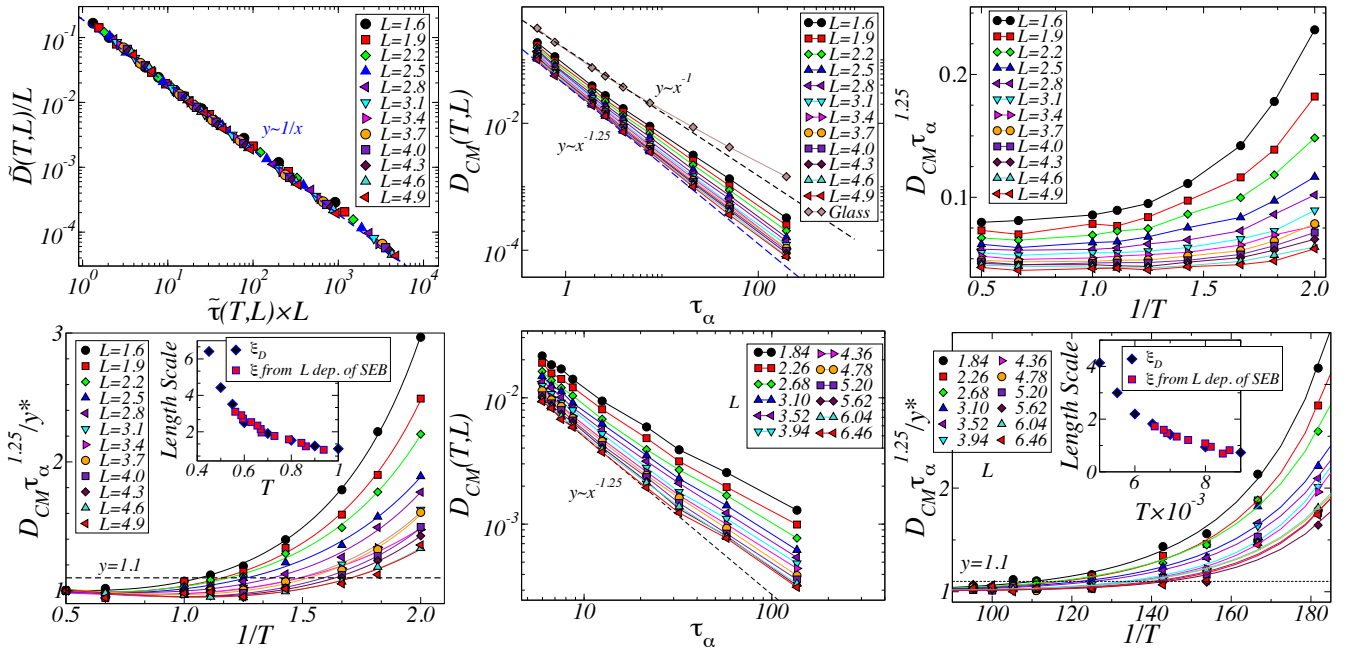


FIG. 4. (a) The cross plot collapse of  $\tilde{D}(T, L)/L$  and  $\tilde{\tau}(T, L) \times L$  for 3dKA liquid shows the validity of the Stokes-Einstein relation for rods' self variables, along with the same rod-length dependence (even with violations because of supercooling). In SI, one can find a similar plot for the 3dHP model. The cross plot between the  $D_{CM}(T, L)$  and the liquids' relaxation time ( $\tau_\alpha(T)$ ) shows the emergent power-law of  $D_{CM} \sim \tau_\alpha^{-1.25}$  in both 3dKA (b) and 3dHP (e) models for large rod lengths. The fractional SE relation  $D_{CM}\tau_\alpha^{1.25} \sim \text{const. of } T$  is checked and found to be violating at lower and lower temperatures for larger rods in (c) for the 3dKA model. The SEB temperature for various rod lengths is obtained as a  $y/y^* = 1.1$  cut to  $y = y^* \exp[x + c_0(x/x_0)^n + c_1(x/x_0)^{2n}]$  functional fit. Here,  $x = 1/T$ ,  $y(T, L) = D_{CM}\tau_\alpha^{1.25}$ , and  $y^*$ ,  $c_0$ ,  $c_1$ ,  $x_0$ ,  $n$  are the fitting parameters. The procedure is strictly followed as in [], and is outlined in (d) and (f) panel for 3dKA and 3dHP models. The rod length dependence of SEB temperature is very similar to the system's dynamic length scale and is shown in the respective inset. The missing plots for the 3dHP model can be found in SI.

of  $k$  (large wavelength). In their case, the  $k$  dependence of SEB temperature was found directly related to dynamic heterogeneity length scale  $\xi_D$ . One can rationalize the similarity to our system by assuming that the rod measures the liquid's response at a length scale comparable to its size. We can then compare it with the results obtained at a wave vector  $k \sim 1/L$ , where  $L$  is the rod length. Motivated by this, we also repeated the analysis reported in Ref.[39] to see whether the rod length dependence of SEB temperature correlates with the temperature dependence of liquid's DH length scale. In Fig.4 bottom-right panel, we have shown such an analysis. To obtain SEB temperature for different rods, one has to take  $1/T$  value at  $y/y^* = 1.1$ , where  $y(T, L) = D_{CM}\tau_\alpha^{1.25}$  and  $y^*(L) = y(2.0, L)$ . This procedure is very similar to the one adopted in Ref.[39] and is outlined in the bottom-right panel of Fig.4. The solid lines in the figure are the fit to function  $\ln(y/y^*) = [x + c_0(x/x_0)^n + c_1(x/x_0)^{2n}]$  where  $x = 1/T$ . The rod length dependence of SEB temperature turns out to be very similar to the system's dynamic length scale, as shown in the inset of Fig.4 bottom-right. We have shown the results obtained for 3dKA and 3dHP models in the bottom left and right panels. The generic nature of the results in different model systems again highlights the robustness of the proposed method to obtain the dynamic heterogeneity length scale for supercooled liquids in simulations.

**Breakdown of Stokes-Einstein-Debye (SEDB):** The rotational dynamics of the probe rod is although independent of translation dynamics but can shape the translational dynamics to a large extent. This makes the study of rotation-translation coupling important in the homogeneous medium itself. On the other hand, with supercooling, the rotational-translational dynamics tend to decouple [3, 7, 8]. Translational diffusion is enhanced compared to the rotational diffusion and the medium's viscosity with supercooling. Similar behaviour is observed in our probe-rods. The detailed characterization of the same can be found in SI. Also, because of the intimate coupling of the rotational and translational properties of probes, one can use them as a proxy to each other. In Fig.5(a), the one-to-one correspondence is made between the rotational relaxation time  $\tau_2^r$  (see SI for definition) and  $D_{CM}$ . The fantastic data collapse is obtained when one plot  $\tau_2^r/I$  with  $I$  being the moment of inertia of the rod against  $\tilde{D}(T)$  for all the rod lengths and temperatures. The data collapse suggests a power-law relation between these two quantities as  $\tau_2^r \sim D_{CM}^{-1.05}$ , with an exponent which is a priori not immediately known to us. This relation also suggests faster translational than rotational motions with increasing supercooling. Since in experiments, the viscosity or the relaxation time of the host liquid along with the rotational relaxation time of probes are quite easy to get, one can study the breakdown of fractional Stokes-

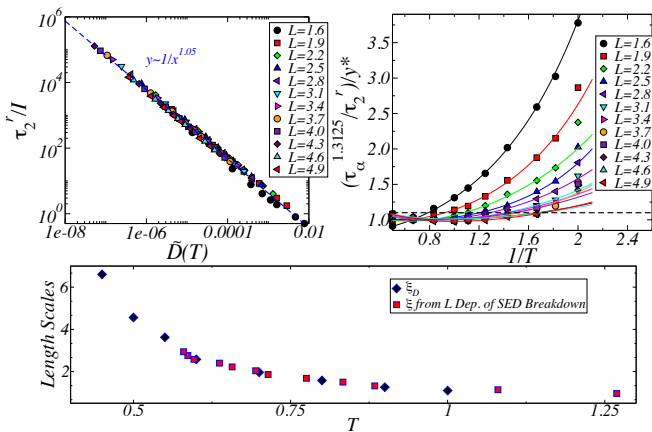


FIG. 5. (a). The 2nd order rotational relaxation time  $\tau_2^r(T, L)$  is plotted against the translational diffusion constant  $\bar{D}_{CM}(T, L)$  to make the one-to-one correspondence between the two. Imposing the SEB analysis on  $\tau_2^r$  would also provide us the growing dynamical correlations in the system. (b). The SEB analysis is done on variable  $\tau_\alpha^{1.3125}/\tau_2^r$  to extract the length scale which is compared with the system's dynamic length scale in (c). This analysis is shown for 3dKA system, similar for the 3dHP model can be found in SI.

Einstein-Debye (SED) to obtain the dynamic length scale as follows. As  $\bar{D}(T) \sim \tau_\alpha^{-\omega}$  in the asymptotic high temperature and large rod length limit, we can expect  $\tau_2^r$  to obey similar power-law relation with  $\tau_\alpha$  as  $\tau_2^r \sim \tau_\alpha^{\omega_r}$  with an exponent  $\omega_r = 1.05\omega \equiv 1.3125$ . We need to plot  $\tau_\alpha^{1.3125}/\tau_2^r$  as a function of  $1/T$  to extract the liquid's dynamical length scale in the same manner before. Fig. 5 (b) & (c) provide the analysis and compare the obtained length scale with  $\xi_D$  for the 3dKA model. A similar analysis for the 3dHP model can be found in SI. The excellent match between the length scale obtained via this analysis and the dynamic length scale,  $\xi_D$  obtained using conventional methods, is remarkably good. This suggests that a complete analysis of Stokes-Einstein and Stokes-Einstein-Debye relation of a probe particle in supercooled liquid medium can unambiguously extract out the growth of underlying dynamic length scale in experimentally relevant glass-forming liquids.

*Experimental Feasibility:* Next, we discuss the experimental feasibility of the proposed method for extracting the dynamic and static length scale in glass-forming liquids. The method presented in this manuscript requires one to record the translational and rotational dynamics of elongated probes of different linear lengths. In Table. I, we have listed some of the existing experimental works that have already measured various rotational and translational quantities of interest for different sized probe molecules in supercooled liquid media. With these existing experimental results, we believe that our proposed method is feasible in experiments without any additional experimental complexity. In fact, our method proposes a simple but direct way to obtain both the dynamic and static length scales of the supercooled liquids from the same experiment.

Medium	Probe	
Glycerol	(a) tbPDI [40, 41]	(b) dpPDI [40]
	(c) dapPDI [40]	(d) Rubrene [42]
	(e) Gold nano-rods [43]	
	(a) Rubrene [44, 45]	(b) BPEA [45]
	(c) Tetracene [44–46]	(d) dpPDI
<i>ortho</i> -terphenyl (OTP)	(e) Anthracene [45, 46]	(f) tbPDI
	(g) egPDI	(h) pPDI [47]
	(i) BODIPY268-dye [48]	

TABLE I. List of probes used to study the dynamics of supercooled Glycerol and OTP in experiments.

*Results & Discussions:* To summarise, we have devised a method to obtain the growing many-body static correlation in a supercooled liquid medium by studying the probe size dependence of averaged translational diffusion constant and relaxation time of rod-like probes. A detailed scaling analysis very nicely rationalizes all the observed results for various temperatures and rod lengths in a unified manner. Similarly, we showed that by studying the Stokes-Einstein relation between the diffusion constants of rods and the medium's relaxation time, one could elegantly extract the growing, dynamic correlation length. This result corroborates very well previous simulation studies on the breakdown of Stokes-Einstein relation in supercooled liquid at various probing wave vectors. Additionally, on considering the self properties of the rod, the Stokes-Einstein relation is found to be obeyed regardless of the rod-length or the degree of supercooling (at least in the studied temperature range), implying the rods' Brownian nature. Next, we expect to have an excellent noise-to-signal ratio from an experimental perspective since the measured quantities are mostly the first moments of various correlation functions. This further translates to the method's usefulness to simultaneously study the growth of static and dynamic correlation lengths in molecular glass-forming supercooled liquids. This method's feasibility in experiments is also immediately apparent with the availability of probe particles of varying sizes and the existing relevant experimental techniques using these probes, albeit mainly for the rotational motion. Thus, a systematic study of these probe particles' translational motions in supercooled liquids would indeed serve our purpose. We end this article with the note that understanding the growth of these length scales in glass-forming molecular liquids is most important as one observes 13 to 14 orders of magnitude of increase in the viscosity or relaxation time while approaching glass transition, unlike in colloidal glasses or in computer simulations where only first 3 to 4 decades of slowing down can be studied.

*Acknowledgement:* This project is funded by intramural funds at TIFR Hyderabad from the Department of Atomic Energy (DAE). Support from Swarna Jayanti Fellowship grants DST/SJF/PSA-01/2018-19 and SB/SFJ/2019-20/05 are also acknowledged.

\* anoopm@tifrh.res.in

† smarajit@tifrh.res.in

- [1] Debenedetti, P. G.; Stillinger, F. H. Supercooled liquids and the glass transition. *Nature* **2001**, *410*, 259–267.
- [2] Dyre, J. C. Colloquium: The glass transition and elastic models of glass-forming liquids. *Reviews of Modern Physics* **2006**, *78*, 953–972.
- [3] Ediger, M. D. Spatially Heterogeneous Dynamics in Supercooled Liquids. *Annual Review of Physical Chemistry* **2000**, *51*, 99–128, PMID: 11031277.
- [4] Karmakar, S.; Dasgupta, C.; Sastry, S. Growing Length Scales and Their Relation to Timescales in Glass-Forming Liquids. *Annual Review of Condensed Matter Physics* **2014**, *5*, 255–284.
- [5] Berthier, L.; Biroli, G. Theoretical perspective on the glass transition and amorphous materials. *Reviews of Modern Physics* **2011**, *83*, 587–645.
- [6] Keys, A. S.; Abate, A. R.; Glotzer, S. C.; Durian, D. J. Measurement of growing dynamical length scales and prediction of the jamming transition in a granular material. *Nature Physics* **2007**, *3*, 260 EP –.
- [7] Blackburn, F. R.; Wang, C.-Y.; Ediger, M. D. Translational and Rotational Motion of Probes in Supercooled 1, 3, 5-Tris(naphthyl)benzene. *The Journal of Physical Chemistry* **1996**, *100*, 18249–18257.
- [8] Edmond, K. V.; Elsesser, M. T.; Hunter, G. L.; Pine, D. J.; Weeks, E. R. Decoupling of rotational and translational diffusion in supercooled colloidal fluids. *Proceedings of the National Academy of Sciences* **2012**, *109*, 17891–17896.
- [9] Weeks, E. R.; Crocker, J. C.; Levitt, A. C.; Schofield, A.; Weitz, D. A. Three-Dimensional Direct Imaging of Structural Relaxation Near the Colloidal Glass Transition. *Science* **2000**, *287*, 627–631.
- [10] Nagamanasa, K. H.; Gokhale, S.; Sood, A. K.; Ganapathy, R. Direct measurements of growing amorphous order and non-monotonic dynamic correlations in a colloidal glass-former. *Nature Physics* **2015**, *11*, 403–408.
- [11] Gokhale, S.; Nagamanasa, K. H.; Ganapathy, R.; Sood, A. K. Growing dynamical facilitation on approaching the random pinning colloidal glass transition. *Nature Communications* **2014**, *5*.
- [12] Berthier, L.; Biroli, G.; Bouchaud, J.-P.; Cipelletti, L.; Masri, D. E.; L'Hôte, D.; Ladieu, F.; Pierno, M. Direct Experimental Evidence of a Growing Length Scale Accompanying the Glass Transition. *Science* **2005**, *310*, 1797–1800.
- [13] Karmakar, S.; Dasgupta, C.; Sastry, S. Growing length and time scales in glass-forming liquids. *Proceedings of the National Academy of Sciences* **2009**, *106*, 3675–3679.
- [14] Karmakar, S.; Dasgupta, C.; Sastry, S. Length scales in glass-forming liquids and related systems: a review. *Reports on Progress in Physics* **2015**, *79*, 016601.
- [15] Adam, G.; Gibbs, J. H. On the Temperature Dependence of Cooperative Relaxation Properties in Glass-Forming Liquids. *The Journal of Chemical Physics* **1965**, *43*, 139–146.
- [16] Kauzmann, W. The Nature of the Glassy State and the Behavior of Liquids at Low Temperatures. *Chemical Reviews* **1948**, *43*, 219–256.
- [17] Biroli, G.; Karmakar, S.; Procaccia, I. Comparison of Static Length Scales Characterizing the Glass Transition. *Phys. Rev. Lett.* **2013**, *111*, 165701.
- [18] Biroli, G.; Bouchaud, J.-P.; Cavagna, A.; Grigera, T. S.; Verrocchio, P. Thermodynamic signature of growing amorphous order in glass-forming liquids. *Nature Physics* **2008**, *4*, 771–775.
- [19] Albert, S.; Bauer, T.; Michl, M.; Biroli, G.; Bouchaud, J.-P.; Loidl, A.; Lunkenheimer, P.; Tourbot, R.; Wiertel-Gasquet, C.; Ladieu, F. Fifth-order susceptibility unveils growth of thermodynamic amorphous order in glass-formers. *Science* **2016**, *352*, 1308–1311.
- [20] Cicerone, M. T.; Douglas, J. F.  $\beta$ -Relaxation governs protein stability in sugar-glass matrices. *Soft Matter* **2012**, *8*, 2983–2991.
- [21] Cicerone, M. T.; Soles, C. L. Fast Dynamics and Stabilization of Proteins: Binary Glasses of Trehalose and Glycerol. *Biophysical Journal* **2004**, *86*, 3836–3845.
- [22] Dirama, T. E.; Carri, G. A.; Sokolov, A. P. Role of hydrogen bonds in the fast dynamics of binary glasses of trehalose and glycerol: A molecular dynamics simulation study. *The Journal of Chemical Physics* **2005**, *122*, 114505.
- [23] Kwon, S.; Cho, H. W.; Kim, J.; Sung, B. J. Fractional Viscosity Dependence of Reaction Kinetics in Glass-Forming Liquids. *Phys. Rev. Lett.* **2017**, *119*, 087801.
- [24] Mukherjee, M.; Mondal, J.; Karmakar, S. Role of  $\alpha$  and  $\beta$  relaxations in collapsing dynamics of a polymer chain in supercooled glass-forming liquid. *The Journal of Chemical Physics* **2019**, *150*, 114503.
- [25] Kaufman, L. J. Heterogeneity in Single-Molecule Observables in the Study of Supercooled Liquids. *Physical Chemistry* **2013**, *64*, 177–200.
- [26] Mutneja, A.; Karmakar, S. Dynamics of Rod like Particles in Supercooled Liquids – Probing Dynamic Heterogeneity and Amorphous Order. 2020.
- [27] Jain, R.; Sebastian, K. L. Diffusing diffusivity: Rotational diffusion in two and three dimensions. *The Journal of Chemical Physics* **2017**, *146*, 214102.
- [28] Chakrabarty, S.; Tah, I.; Karmakar, S.; Dasgupta, C. Block Analysis for the Calculation of Dynamic and Static Length Scales in Glass-Forming Liquids. *Phys. Rev. Lett.* **2017**, *119*, 205502.
- [29] Bhowmik, B. P.; Tah, I.; Karmakar, S. Non-Gaussianity of the van Hove function and dynamic-heterogeneity length scale. *Physical Review E* **2018**, *98*.
- [30] Kob, W.; Andersen, H. C. Testing mode-coupling theory for a supercooled binary Lennard-Jones mixture I: The van Hove correlation function. *Phys. Rev. E* **1995**, *51*, 4626–4641.
- [31] O’Hern, C. S.; Langer, S. A.; Liu, A. J.; Nagel, S. R. Random Packings of Frictionless Particles. *Phys. Rev. Lett.* **2002**, *88*, 075507.
- [32] Mermin, N. D.; Wagner, H. Absence of Ferromagnetism or Antiferromagnetism in One- or Two-Dimensional Isotropic Heisenberg Models. *Phys. Rev. Lett.* **1966**, *17*, 1133–1136.
- [33] Illing, B.; Fritsch, S.; Kaiser, H.; Klix, C. L.; Maret, G.; Keim, P. Mermin–Wagner fluctuations in 2D amorphous solids. *Proceedings of the National Academy of Sciences* **2017**, *114*, 1856–1861.
- [34] Mazoyer, S.; Ebert, F.; Maret, G.; Keim, P. Dynamics of particles and cages in an experimental 2D glass former. *EPL (Europhysics Letters)* **2009**, *88*, 66004.
- [35] Chakrabarty, S.; Das, R.; Karmakar, S.; Dasgupta, C. Understanding the dynamics of glass-forming liquids with random pinning within the random first order transition theory. *The Journal of Chemical Physics* **2016**, *145*, 034507.
- [36] Li, Y.-W.; Mishra, C. K.; Sun, Z.-Y.; Zhao, K.; Mason, T. G.; Ganapathy, R.; Ciamarra, M. P. Long-wavelength fluctuations and anomalous dynamics in 2-dimensional liquids. *Proceedings of the National Academy of Sciences* **2019**, *116*, 22977–22982.
- [37] Doi, M.; Edwards, S. F. *The theory of polymer dynamics*; International series of monographs on physics 73; Clarendon Press:

- Oxford, 2007.
- [38] Landau, L. D. *Fluid Mechanics: Landau and Lifshitz: Course of Theoretical Physics, Volume 6*; Pergamon, 2013.
- [39] Parmar, A. D.; Sengupta, S.; Sastry, S. Length-Scale Dependence of the Stokes-Einstein and Adam-Gibbs Relations in Model Glass Formers. *Physical Review Letters* **2017**, *119*.
- [40] Mackowiak, S. A.; Leone, L. M.; Kaufman, L. J. Probe dependence of spatially heterogeneous dynamics in supercooled glycerol as revealed by single molecule microscopy. *Phys. Chem. Chem. Phys.* **2011**, *13*, 1786–1799.
- [41] Zondervan, R.; Kulzer, F.; Berkhout, G. C. G.; Orrit, M. Local viscosity of supercooled glycerol near  $T_g$  probed by rotational diffusion of ensembles and single dye molecules. *Proceedings of the National Academy of Sciences* **2007**, *104*, 12628–12633.
- [42] Mackowiak, S. A.; Herman, T. K.; Kaufman, L. J. Spatial and temporal heterogeneity in supercooled glycerol: Evidence from wide field single molecule imaging. *The Journal of Chemical Physics* **2009**, *131*, 244513.
- [43] Yuan, H.; Khatua, S.; Zijlstra, P.; Orrit, M. Individual gold nanorods report on dynamical heterogeneity in supercooled glycerol. *Faraday Discussions* **2013**, *167*, 515.
- [44] Cicerone, M. T.; Ediger, M. D. Relaxation of spatially heterogeneous dynamic domains in supercooled ortho-terphenyl. *The Journal of Chemical Physics* **1995**, *103*, 5684–5692.
- [45] Cicerone, M. T.; Ediger, M. D. Enhanced translation of probe molecules in supercooled o-terphenyl: Signature of spatially heterogeneous dynamics? *The Journal of Chemical Physics* **1996**, *104*, 7210–7218.
- [46] Cicerone, M. T.; Ediger, M. D. Photobleaching technique for measuring ultraslow reorientation near and below the glass transition: tetracene in o-terphenyl. *The Journal of Physical Chemistry* **1993**, *97*, 10489–10497.
- [47] Leone, L. M.; Kaufman, L. J. Single molecule probe reports of dynamic heterogeneity in supercooled ortho-terphenyl. *The Journal of Chemical Physics* **2013**, *138*, 12A524.
- [48] Paeng, K.; Park, H.; Hoang, D. T.; Kaufman, L. J. Ideal probe single-molecule experiments reveal the intrinsic dynamic heterogeneity of a supercooled liquid. *Proceedings of the National Academy of Sciences* **2015**, *112*, 4952–4957.



# Translational Dynamics of Rod-like Particles in Supercooled Liquids : Probing Dynamic Heterogeneity and Amorphous Order- Supplemental Material

Anoop Mutneja\* and Smarajit Karmakar†  
 Tata Institute of Fundamental Research, 36/P, Gopanpally Village,  
 Serilingampally Mandal, Ranga Reddy District, Hyderabad, 500107, Telangana, India

## Contents

<b>I. Definitions/Methods</b>	1
A. van Hove Function	1
B. Overlap correlation function $Q(t)$ & Structural relaxation time $\tau_\alpha$	2
C. Four-Point Susceptibility $\chi_4(t)$	3
D. Point-to-Set Method	3
<b>II. Translational of center of mass (CoM) of probe rods in supercooled liquids:</b>	3
A. MSD of CoM of probe rods	3
B. Diffusion constants of CoM of probe rods	5
C. Translational relaxation of CoM of rod	6
<b>III. Stokes-Einstein Relations</b>	6
<b>IV. Rotational Quantities</b>	9
A. Rotational correlation function	9
B. Rotational Non-Normal Parameter	9
<b>V. Stokes-Einstein-Debye Relation</b>	9
<b>VI. Existing experimental studies</b>	11
<b>VII. Model Systems &amp; simulation details</b>	12
<b>References</b>	13

## I. DEFINITIONS/METHODS

### A. van Hove Function

The van Hove distribution function,  $G(\mathbf{r}, t)$ , is the dynamical correlation function. It provides us the correlation between two particles separated by distance  $r$  and time  $t$ . It is defined as the probability density of particle ' $i$ ' at position ' $\mathbf{r}$ ' and time ' $t$ ', with the prior knowledge of particle ' $j$ ' being at the origin at an initial time.

$$G(\mathbf{r}, t) = \frac{1}{N} \left\langle \sum_{i=1}^N \sum_{j=1}^N \delta(\mathbf{r} - (\mathbf{r}_i(t) - \mathbf{r}_j(0))) \right\rangle \quad (1)$$

The self part of the van Hove function,  $G_s(\mathbf{r}, t)$ , is the most commonly used quantity and is defined as the probability of finding a particular particle at position ' $\mathbf{r}$ ' and time ' $t$ ' when it is known to be at origin initially. This can also be simply thought of as

\*Electronic address: anoopm@tifrh.res.in

†Electronic address: smarajit@tifrh.res.in

the distribution of the displacements of the particles at a given time  $t$ . It is formally defined as

$$G_s(\mathbf{r}, t) = \frac{1}{N} \left\langle \sum_{i=1}^N \delta(\mathbf{r} - (\mathbf{r}_i(t) - \mathbf{r}_i(0))) \right\rangle. \quad (2)$$

For a Brownian particle, the self part is thus given by the following expression, which would also be valid for particles in any homogeneous diffusive system at a large enough distance and long enough timescales,

$$G_s(\mathbf{r}, t) = \frac{1}{(4\pi Dt)^{3/2}} \exp\left(-\frac{r^2}{4Dt}\right). \quad (3)$$

Here  $D$  is the diffusion constant of the system. Thus for such a Gaussian process the measure of dynamical heterogeneity in a disordered system will simply be the non-Gaussianity of  $G_s(\mathbf{r}, t)$  at that time, implying the Binder cumulant,  $\alpha_2(t)$ . The  $\alpha_2(t)$  is defined as

$$\alpha_2(t) = 1 - \frac{\langle |\mathbf{r}|^4 \rangle}{3 \langle |\mathbf{r}|^2 \rangle^2}. \quad (4)$$

The dynamical correlation between different particles is best measured by the distinct part of van Hove function and is defined by considering different  $i$  and  $j$  particles in Eq.1.

### B. Overlap correlation function $Q(t)$ & Structural relaxation time $\tau_\alpha$

The overlap function,  $Q(t)$  gives the measure of overlap between two configurations separated by time interval ‘ $t$ ’ and is defined as follows:

$$Q(t) = \frac{1}{N} \sum_{i=1}^N \theta(a - |\mathbf{r}_i(t) - \mathbf{r}_i(0)|) \quad (5)$$

Here,  $\theta(x)$  is the usual step function, and the value of  $a$  is chosen to ignore the decorrelation that might happen due to particles’ vibrational motion in their cages. In Fig.1, we have plotted the  $Q(t)$  for the rod of length  $L = 2.5$  &  $L = 3.1$  immersed in 3dKA (left-panel) & 3dHP (right-panel) system, respectively, at different temperatures. The two step relaxation can be very clearly seen from the figures. The structural relaxation time  $\tau_\alpha$  is defined in terms of overlap function. It is the time when the average

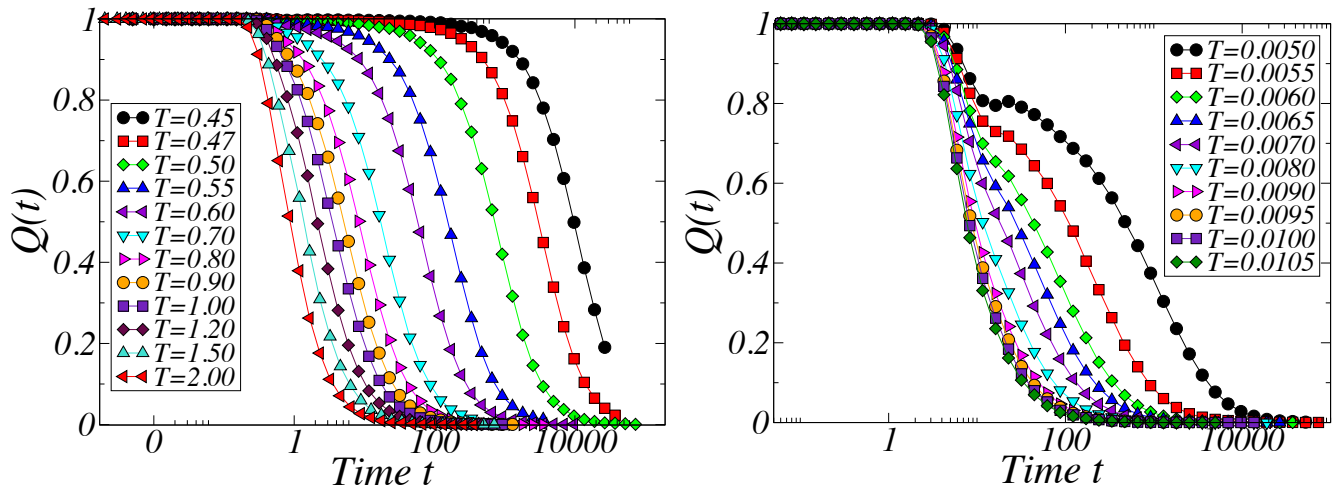


FIG. 1: Left-Panel: The overlap correlation function,  $Q(t)$  for the rod of length  $L = 2.5$  immersed in the 3dKA model liquid at different temperatures. Right-Panel: The time evolution of  $Q(t)$  for the rod of length  $L = 3.1$  immersed in the 3dHP model liquid at different temperatures.

value of the overlap function reduces to  $1/e$ , i.e.,  $\langle Q(\tau_\alpha) \rangle = 1/e$ . Note that the temperature dependence of  $\tau_\alpha$  doesn’t depend on the particular choice of the parameter  $a$ . Parameter  $a$  is chosen to remove any possible decorrelation that might come due to vibrations of these particles in their respective cages formed by the neighbours.

### C. Four-Point Susceptibility $\chi_4(t)$

Four-Point Susceptibility,  $\chi_4(t)$  [1, 2] is calculated as the variance or fluctuation of two point density correlation function or the overlap function,  $Q(t)$ . The variance of overlap function at time  $t$  will be the measure of fluctuation in relaxation in the system at that particular time due to dynamic heterogeneity. It is defined as

$$\chi_4(t) = N \left[ \langle Q^2(t) \rangle - \langle Q(t) \rangle^2 \right]. \quad (6)$$

At short times  $Q(t)$  is very close to 1 and goes to zero at larger times so one expects that  $\chi_4(t)$  will be small (close to zero) at very short and long times thus there will be a peak at some intermediate timescales. This timescales is found to be very close to the  $\alpha$ -relaxation time,  $\tau_\alpha$ . This suggests that heterogeneity is maximum at the structural relaxation time.

### D. Point-to-Set Method

The causal relation between the growing viscosity of the supercooled liquid and the growing length scale of the mosaic state has been advocated in the RFOT theory. The more physical way to understand this length scale is in terms of Point-to-set (PTS) correlation function. One can gain the theoretical perspective about PTS length scale,  $\xi_{PTS}$  in Ref.[3]. PTS length scale is calculated by taking a well equilibrated configuration of the system and then freezing all the particles outside a region  $\mathcal{C}$  of linear dimension  $\xi$  as a boundary condition. The particles inside  $\mathcal{C}$  are then relaxed and overlap function with the initial configuration is calculated. For small enough  $\xi$  overlap should be very high implying that the particles inside can remain restricted to the same equilibrium state. But on increasing the  $\xi$  the overlap would start to decrease and vanish, eventually. Physically, it is because of the fact that this large enough volume can not hold itself to single metastable state. The largest linear length scale  $\xi = \xi_{PTS}$  to which volume of particles can be restricted to same metastable minimum is known as PTS length scale. This means that the mosaic of this linear dimension can survive in particular metastable state, and thus whole system can be thought of as divided into such mosaics of metastable states. The length scale obtained in this way is found to be same as static length scale obtained by finite size scaling of  $\tau_\alpha$ [4] and from minimum eigenvalue of Hessian matrix [5].

## II. TRANSLATIONAL OF CENTER OF MASS (COM) OF PROBE RODS IN SUPERCOOLED LIQUIDS:

Anisotropy in the translation of CoM of rod in the homogeneous liquid is evident as a rod tends to have a larger diffusion constant in the direction of its orientation ( $D_{\parallel}$ ) than any of the perpendicular direction ( $D_{\perp}$ ). But eventually, with rotational decorrelation, this anisotropy disappears with time. The translation of CoM of rods is not a Gaussian process because of the strong rotation-translation coupling. It becomes Gaussian when the relevant length scale (diffusion length) becomes much larger than rod length. Readers are encouraged to read chapter-8 of the book [6] for more details. This section will discuss effects of supercooling and rod length on various translational quantities of probe rods. The first things that will be discussed are the mean squared displacement (MSD), anisotropy observed in diffusion along and perpendicular to the rod, translational overlap function  $Q_{CM}(t, T, L)$ , and the relaxation time associated, etc.

### A. MSD of CoM of probe rods

The mean squared displacement (MSD) of CoM of the rod is defined as,

$$MSD = \langle |\mathbf{r}_{CM}(t) - \mathbf{r}_{CM}(0)|^2 \rangle = \langle |\Delta \mathbf{r}_{CM}|^2 \rangle \quad (7)$$

Where  $\mathbf{r}_{CM}(t)$  is the CoM position vector at a time ' $t$ '. Fig.2 (left panel) is the time evolution of MSD for the rod of fixed length ( $L = 2.5$ ) immersed in a liquid (3dKA model) at various temperatures in the supercooled regime. In this figure's center panel, the rod length variation of MSD is shown for probe rod in 3dKA liquid at  $T = 0.60$ . For comparison, the MSD of parent liquid particles is also included in this plot.

Following are few remarks one can make from these plots. Firstly, rod's caging duration increases with the supercooling, as expected. Secondly, the larger rods diffuse more slowly than, the smaller ones and the parent liquid particles. The caging duration doesn't change much with the increase in rod length at a given temperature which can be rationalized easily, at least for the diffusion parallel to the rod length since it will depend mainly on the crowding near the tip of the rod. Thus, it will be mostly a function of the medium's density. Also, since the rotational correlations for large enough rods can survive for substantially long times in supercooled liquids, the MSD of CoM of the rod along the rod's initial orientation and the components perpendicular to it, would provide us insight into the translational anisotropy of the probe rods. Fig.2 (right panel) contains the plots for the time

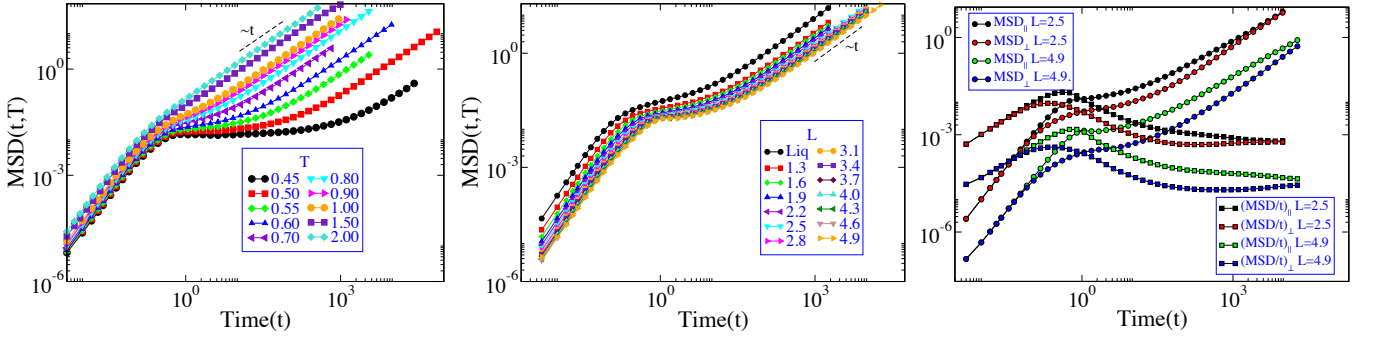


FIG. 2: Left panel: The time evolution of MSD of rod's CoM with  $L = 2.5$  immersed in 3dKA medium at various supercooling temperatures. Center panel: The MSD evolution plot for different sized probes in 3dKA liquid at temperature  $T = 0.6$ , for comparison with the parent liquid, MSD of liquid particles is also included in the plot. Right panel: Evolution of parallel and perpendicular components of MSD of rod (circles) for small ( $L = 2.5$ ) and large rods ( $L = 4.9$ ) and the corresponding  $MSD/t$  (square symbols) components which in long time limit are proportional to the diffusion constant. The more diffusion along the rod can be clearly seen at the initial and intermediate times but as the rod rotationally decorrelates at long times, the MSD along both directions coincides (see text for more discussion).

evolution of the MSD (circle symbols) component parallel to the initial orientation and the orthogonal component. These plots are for rod of size  $L = 2.5$  (small) and  $L = 4.9$  (large) immersed in 3dKA liquid at  $T = 0.60$  temperature. One can see that the ballistic time duration lasts longer for the parallel component, which can be justified from geometrical arguments. Also, at large times, both the components should diffuse equally because of the rotational decorrelation, which can be easily speculated.

In contrast, during the intermediate times, the diffusion along the rod length is larger, consistent with the expected behaviour [6]. The square symbols in Fig.2 (right-panel) represent the MSD per unit time which is linked to the diffusion constant. One can see that the parallel component diffuses faster but eventually would come around to other components as the rod relaxes rotationally. The parallel and perpendicular part of MSD is defined as,

$$MSD_{||} = \langle |\Delta \mathbf{r}_{CM} \cdot \hat{\mathbf{u}}_0|^2 \rangle \quad (8)$$

$$MSD_{\perp} = 0.5 \langle |\Delta \mathbf{r}_{CM}|^2 - |\Delta \mathbf{r}_{CM} \cdot \hat{\mathbf{u}}_0|^2 \rangle, \quad (9)$$

where  $\hat{\mathbf{u}}_0$  is the orientation vector of the rod at time  $t = 0$ . There is a half multiplied to the perpendicular component to account for two independent orthogonal directions.

*Rod-length dependence of  $MSD_{||}$  and  $MSD_{\perp}$ :* The Brownian particle's diffusion constant in a homogeneous medium is

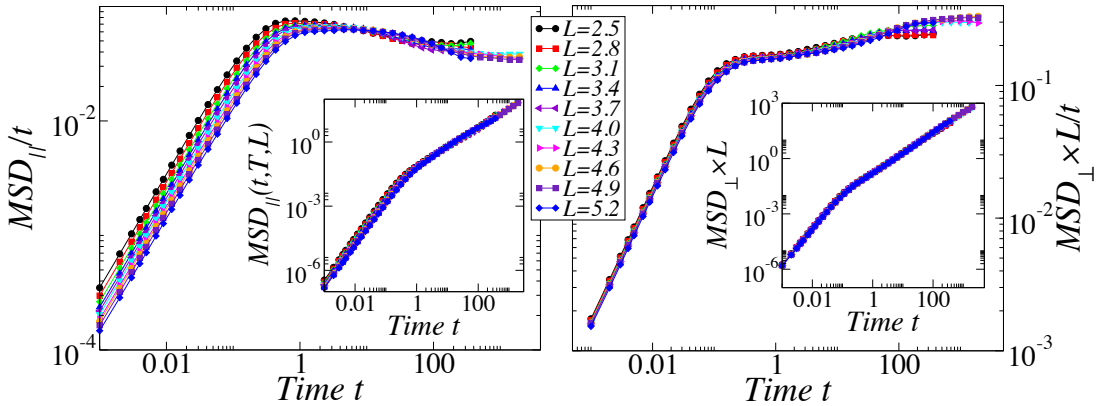


FIG. 3: Left Panel: The time evolution of  $MSD_{||}(t)$  per unit time is shown, along with the  $MSD_{||}(t)$  itself in the inset, for rods of various lengths in 3dKA medium at  $T = 2.0$  (high-temperature). The plot serves the purpose of illustrating the no rod length dependence on the parallel diffusion of rod, until the rotational decorrelation kicks in. Right Panel: The similar plot of the  $MSD_{\perp} \times L$  per unit time illustrates the  $1/L$  rod-length scaling of the perpendicular component, until the rotational decorrelation make the translation equivalent in each direction.

inversely related to its hydrodynamic radius  $R_H$ . For a spherical particle, the hydrodynamic radius is the same as its radius. For the rod-like particles, the hydrodynamic radius scales as  $R_H \sim \frac{L}{\log(L/\sigma+b)}$  [6]. Here,  $L$  is the rod's length,  $\sigma$  is the rod's width, and  $b$  is the constant to account for the end effects. This expression for  $R_H$  explains the rod-length scaling of the rod's

CoM' diffusion constant and the relaxation time (discussed in the next section). Apart from this, the  $MSD_{\parallel}$  and  $MSD_{\perp}$  would depend on rod length in a very different way. The parallel component should see the liquid from a view of the rod's diameter, i.e.,  $\sigma$ . Thus, it should not depend on rod length at all. One can see in Fig.3 (left-panel), the  $MSD_{\parallel}$  and  $MSD_{\parallel}/t$  collapse automatically for different rod-lengths in the 3dKA system at temperature  $T = 2.0$ . On the other hand, the orthogonal component should see the liquid as a spherical particle of diameter  $L$ , implying the MSD should be scalable by  $1/L$ , as seen in Fig.1(right-panel).

### B. Diffusion constants of CoM of probe rods

Translation diffusion constant ( $D_{CM}$ ) for the CoM of the rod can be obtained from MSD using an expression  $D_{CM}(T, L) = MSD(t \rightarrow \infty, T, L)/6t$ . Temperature variation of  $D_{CM}$  for rods of various lengths in 3dKA (and 3dHP) liquid and its rod length variation for rods in different temperature liquid is plotted in the top-left and top-center panel of Fig.4 (and Fig.5), respectively. As discussed in the previous section and in the main text, the diffusion constant for a Brownian rod should follow the  $\ln(L/\sigma + b_1)/L$  dependence with  $b_1$  being a constant. Fig.4 & 5 (top-center panel) clearly validate the scaling for rods in high temperature 3dKA & 3dHP liquid. Also, In the top-right panel of the respective figures, we removed this asymptotic rod length dependence by plotting  $\tilde{D}(T, L) = D_{CM}L/\ln(L/\sigma + b_1)$  w.r.t. rod length. In our models,  $\sigma = 1.0$ , and the value of  $b_1$  is obtained by fitting the high-temperature data. One can clearly see the effect of supercooling in play, the diffusion-constant,  $\tilde{D}$  starts to deviate from the constant value at larger and larger rod length with increasing supercooling. This indicates the growth of some underlying length-scale. The deviation here implies the faster diffusion of the smaller rods, while the larger rods still feel the liquid as a homogeneous medium. As argued in the main text and in Ref. [7], this increase of deviation in  $\tilde{D}$  from its constant high temperature and large rod length value with decreasing probe-length is linked to the parent liquid's correlated relaxation processes, the linear-length of which gives the static length scale of the system. In Fig.4 & 5 (bottom-left panel) we scaled  $\tilde{D}$  by its large rod-length value at each temperature, i.e.,  $\tilde{D}^*(T) = \tilde{D}(T, L \rightarrow \infty)$ . This data is then collapsed to obtain

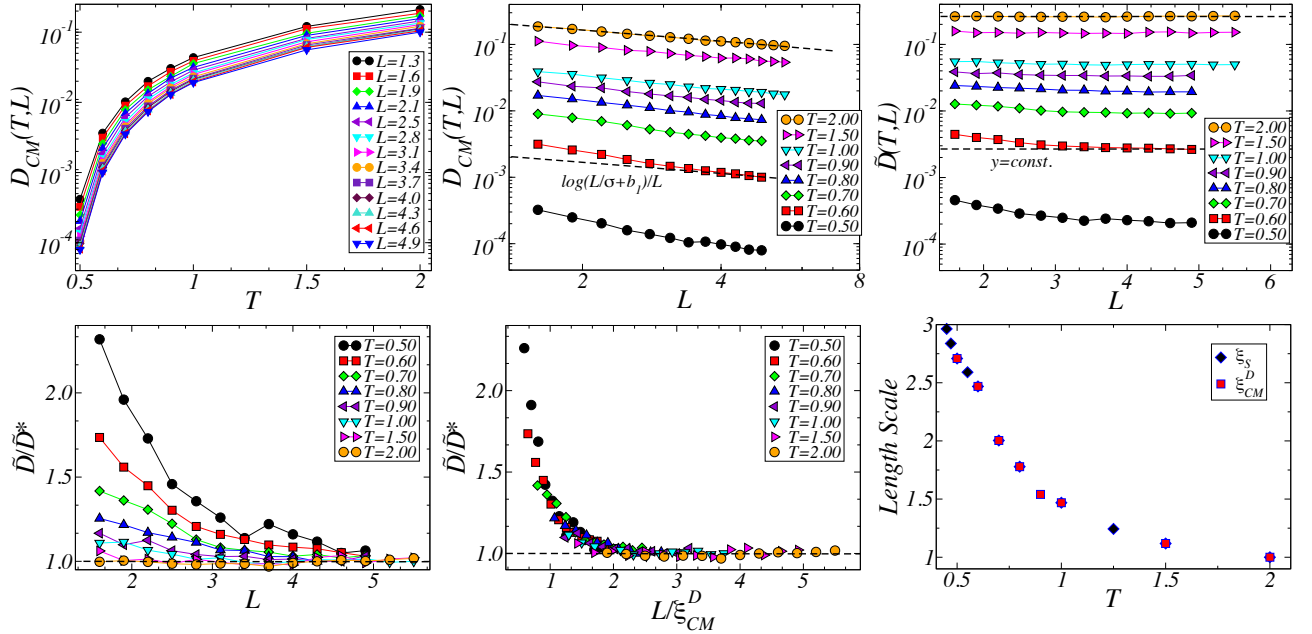


FIG. 4: Top-left panel: Temperature variation of diffusion constant of CoM of rod,  $D_{CM}$  for rod of various lengths immersed in a liquid modelled by 3dKA model. In the top-center panel, the rod length dependence of  $D_{CM}$  for different temperatures is plotted. The Brownian scaling of  $D_{CM} \sim \log(L/\sigma + b_1)/L$  fits the large temperature and large rod-length bits, perfectly. The fitted constant  $b_1$  turns out to be,  $b_1 = 1.49$  with  $\sigma = 1.00$  (width of the rod). This normal liquid scaling is removed by plotting  $\tilde{D}(T, L)$  (defined in text) in top-right panel to observe the supercooling effect. With increasing supercooling the larger and larger rods couldn't survive the emerging structural correlations. In the bottom-left panel the  $\tilde{D}/\tilde{D}^*$  is plotted, where  $\tilde{D}^*$  is the large rod-length asymptotic value of  $\tilde{D}$ . Here the effect of supercooling can be clearly seen, its interpretation is given in text.  $\tilde{D}/\tilde{D}^*$  is collapsed (bottom-center) to obtain the underlying growing length scale,  $\xi_{CM}^D$  (bottom-right). The temperature dependence of  $\xi_{CM}^D$  is also compared with the static length scale of the system  $\xi_S$ , obtained as PTS length scale.



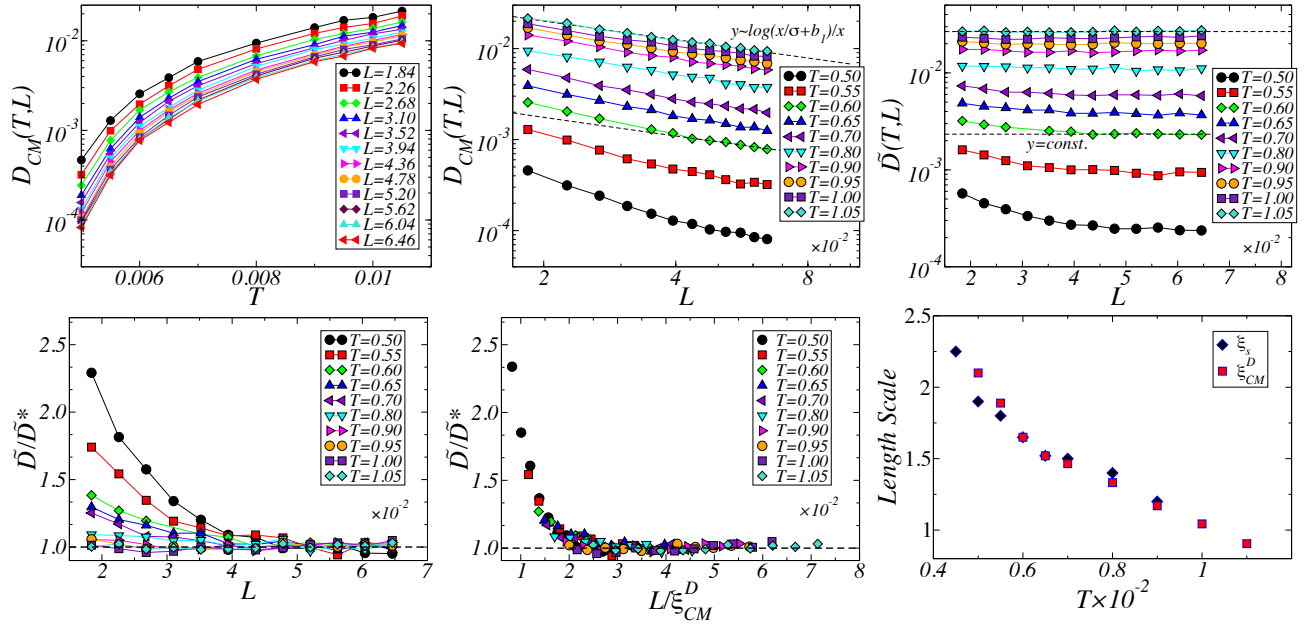


FIG. 5: Similar quantities are plotted as in Fig.4 for the 3dHP model to reach similar conclusions. The fitting constant  $b_1$  turns out to be  $b_1 = 2.05$

the underlying length scale ( $\xi_{CM}^D$ ) using the following scaling ansatz.

$$\frac{\tilde{D}(T, L)}{\tilde{D}^*(T)} = \mathcal{F}\left(\frac{L}{\xi_{CM}^D}\right) \quad (10)$$

The collapse and the comparison of obtained length scale with the static length scale obtained via PTS correlation method is shown in Fig.4 & 5 (bottom-center, right panel) for 3dKA and 3dHP model system, respectively. The quality of collapse and the astonishing similarity in the temperature dependence of obtained length-scale with a static length scale of liquid prove the procedure's robustness. The whole procedure is summed-up in Figs.4 & 5 for 3dKA and 3dHP models respectively.

### C. Translational relaxation of CoM of rod

The translational relaxation time of a rod is defined as the time when overlap function,  $Q(t)$  for CoM of a rod (Eq:5) reduces to  $1/e$ , i.e.,  $\langle Q(t = \tau_{CM}) \rangle = 1/e$ . In Fig.1,  $Q(t)$  is plotted for rod of length  $L = 2.5$  &  $L = 3.1$  immersed in the 3dKA & 3dHP liquid at different temperatures. Temperature dependence of  $\tau_{CM}$  for various sized rods and its rod length dependence in the 3dKA (3dHP) liquid at different temperatures can be found in the left and center panel of Fig.6 (Fig.7) respectively. The rod length scaling of  $\tau_{CM}(T, L)$  should be inverse to that of  $D_{CM}$ , thus following the similar route as to extract the static length scale from diffusion constant, we can obtain the static length scale. The quantity of interest here would be,  $\tilde{\tau}(T, L) = \tau_{CM} \ln(L/\sigma + b_2)/L$ , which would be scaled by large rod-length value at each temperature i.e.,  $\tilde{\tau}^*(T) = \tilde{\tau}(T, L \rightarrow \infty)$ . Then on using the following scaling ansatz the relevant length scale ( $\xi_{CM}^\tau$ ) would be extracted.

$$\frac{\tilde{\tau}(T, L)}{\tilde{\tau}^*(T)} = \mathcal{F}\left(\frac{L}{\xi_{CM}^\tau}\right) \quad (11)$$

This procedure is outlined in Fig.6 & 7 for 3dKA and 3dHP model system.

## III. STOKES-EINSTEIN RELATIONS

The Stokes-Einstein (SE) relation is a blend of Einstein's work on diffusion for spherical particles and Stokes's study on drag felt by a spherical body through the viscous medium, and it reads as,

$$D = \frac{k_B T}{c\pi R\eta} \quad (12)$$

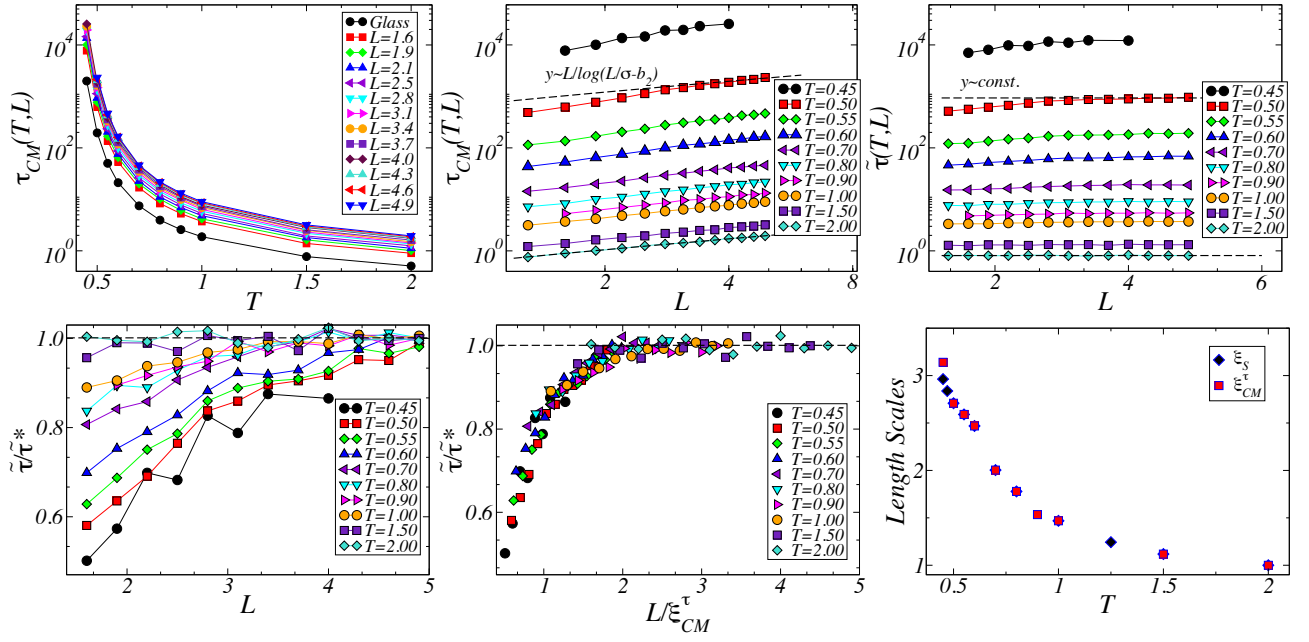


FIG. 6: The temperature dependence and the rod-length dependence of translational relaxation time,  $\tau_{CM}(T, L)$  for rod of different lengths and rods in different temperature 3dKA model are plotted in top-left and top-right panels, respectively. The Brownian rod length dependence of  $\tau_{CM} \sim L/\log(L/\sigma + b_2)$ , is well obeyed for the high temperature liquid and for larger rod-length. The fitting parameter  $b_2$ , turns out to be  $b_2 = 2.67$  with  $\sigma = 1.0$  being the width of the rod.  $\tilde{\tau}(T, L)$  is then plotted in the top-right panel with this scaling removed, i.e.,  $\tilde{\tau} = \tau_{CM} \times \frac{\log(L/\sigma + b_2)}{L}$ . Any deviation from  $\tilde{\tau}(T, L) = f(T)$  is an effect of supercooling. In bottom-left panel,  $\tilde{\tau}/\tilde{\tau}^*$  is plotted, where  $\tilde{\tau}^*(T)$  is the large rod-length asymptote value of  $\tilde{\tau}(T, L)$ . This quantity is then collapsed in the bottom-middle panel to obtain the underlying growing structural order ( $\xi_{CM}^D$ ). Temperature dependence and its comparison with the system's static length scale obtained as PTS length scale is presented in the bottom right panel.

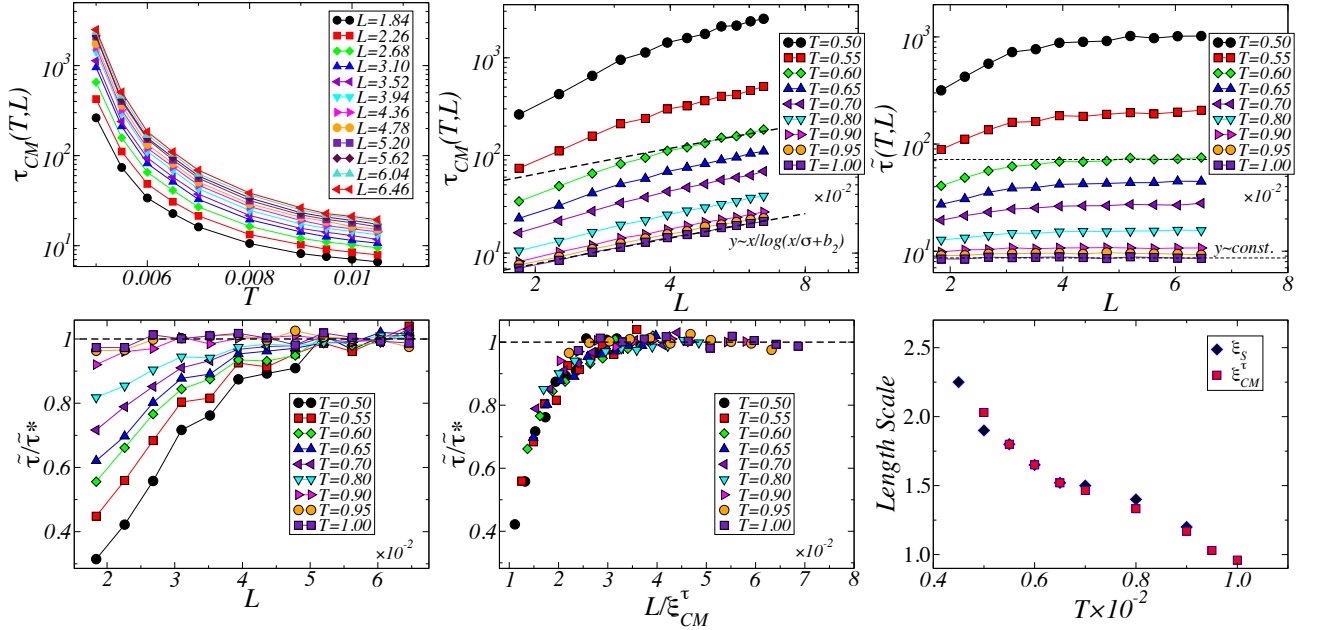


FIG. 7: Similar quantities are plotted as of Fig.6 for 3dHP model to reach similar conclusions. The fitting constant  $b_2$  turns out to be  $b_2 = 6.10$ .

where  $D$  and  $R$  respectively are the diffusion constant and the hydrodynamic radius of the particle,  $\eta$  and  $T$  are the shear viscosity, and the temperature of liquid respectively, and  $c$  is a constant which depends on the boundary condition at the surface of the particle ( $c = 6$  for stick &  $c = 4$  for slip) [8]. This expression is also valid for the liquid particle's self-diffusion,

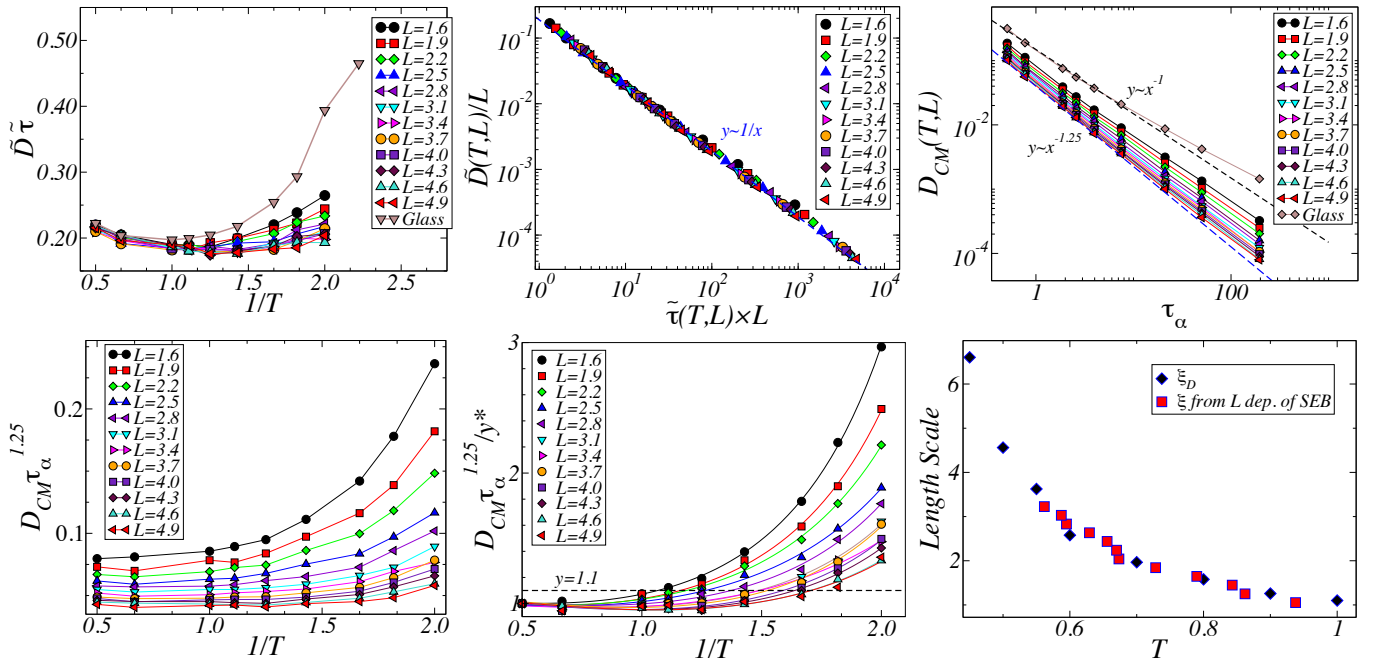


FIG. 8: Top panel: In the left, scaled SE parameter  $\tilde{D}\tilde{\tau}$  is plotted with increasing supercooling for different rod lengths along with the similar SE parameter plot for parent liquid. The non-violation of this SE parameter is displayed best in the center panel with cross plot of  $\tilde{D}/L$  and  $\tilde{\tau} \times L$ . In the right panel similar cross plot between  $D_{CM}$  and  $\tau_\alpha$  suggests the power law of  $D_{CM} \sim \tau_\alpha^{-1.25}$  emerging for large rods and high temperature. Bottom panel: The fractional SE parameter  $D_{CM}\tau_\alpha^{1.25}$  is plotted in the left panel for different rods with respect to inverse temperature. The SEB for this parameter happens at lower and lower temperature for larger rods. The SEB temperature for a particular rod length is chosen to be the temperature when  $D_{CM}\tau_\alpha^{1.25}/y^* = 1.1$ , while this quantity is equal to unity for high temperature. This is outlined in center panel of the figure with solid lines are fit to the function mentioned in text. The obtained rod length dependence for SEB temperature is compared with dynamic length scale of the liquid in right panel.

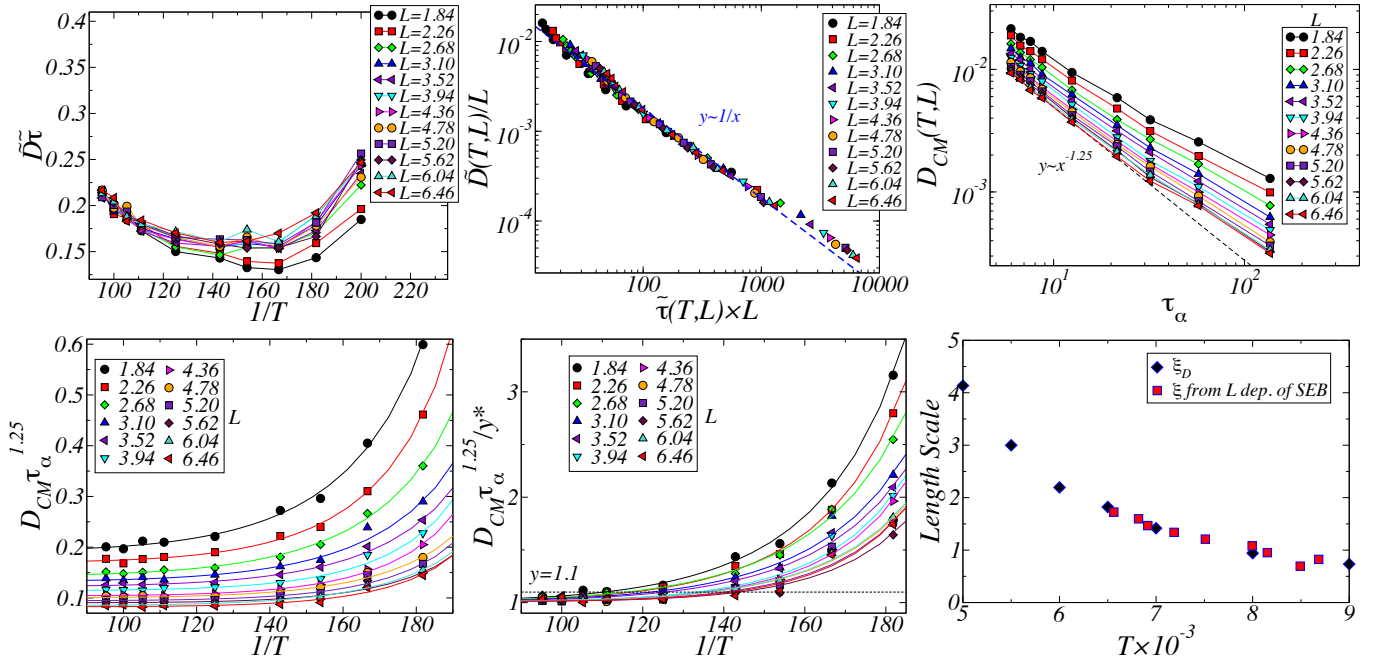


FIG. 9: Similar quantities are plotted as in Fig.8 for 3dHP model system.

and Stokes-Einstein-Breakdown (SEB) is extensively studied as a possible effect of the presence of dynamic heterogeneity in

the system. Since the distribution of local viscosity (structural relaxation time) gets broader due to dynamic heterogeneity, the diffusion constant's growth becomes faster than the predicted value from the SE relation. In this mathematical equation, viscosity is often replaced by relaxation time ( $\eta \sim \tau$ ) or temperature times relaxation time ( $\eta \sim \tau T$ ) as they have very similar temperature dependence at least deep in the supercooled temperature regime where viscosity grows very rapidly with small change in temperature. The first one grounds its correctness in Maxwell relation, i.e.,  $\eta = G_\infty \tau$  where  $G_\infty$  is the instantaneous shear modulus. So the interchangeability of viscosity and relaxation time relies on the assumption of  $G_\infty$  being temperature independent, but it can have some temperature dependence after all. The second relation comes from the Gaussian solution of the diffusion equation, which links the diffusion constant with relaxation time as  $D_t k^2 = 1/\tau_t$ , where  $k$  is the wave vector associated with the self-intermediate scattering function. Both of these proxies are well studied in the literature, and one can find their comparison in [9], but since we would be using SE relation for rods (more Brownian-like behaviour), the choice  $\eta \sim \tau T$  seems more physical. Thus the Stokes-Einstein relation reads out,

$$D\tau = \frac{1}{c\pi R} = f(R). \quad (13)$$

$f(R)$  can be considered as a measure of SEB. For rods in liquid, we can have  $D_{CM}\tau_{CM}$  and  $D_{CM}\tau_\alpha$  as SEB parameters where, as defined earlier,  $D_{CM}$  &  $\tau_{CM}$  is the diffusion constant and relaxation time of CoM of the rod, and  $\tau_\alpha$  is the relaxation time of liquid. Fig. 8 & Fig.9 top-left panel shows the temperature variation of  $\tilde{D}\tilde{\tau}$  for different sized rods. As expected from the previous scaling analysis of  $D_{CM}$  and  $\tau_{CM}$ , that product of  $\tilde{D}\tilde{\tau}$  would be a scaling function of the static length scale (using Eq. 10 & Eq.11). It turns out that scaling functions that govern the rod length dependence of  $\tilde{D}$  and  $\tilde{\tau}$  are inverse of each other. Thus  $\tilde{D}\tilde{\tau}$  will be constant. The smallness of the extent of breakdown can be seen in Fig.8 & Fig.9's top-center panel (3dKA & 3dHP), where  $\tilde{D} \sim \tilde{\tau}$  for a given rod length is confirmed in their cross plot. A similar cross plot between  $D_{CM}$  and  $\tau_\alpha$  is also included in the top-right panel of the same figure, which predicts a different power law of  $D_{CM} \sim \tau_\alpha^{-1.25}$  for high temperature and large rods. As pointed out in the main text, the temperature of departure from this power-law or the SEB temperature for a different rod length behaves like the dynamic length scale of the system [10]. This procedure, in complete depth, is illustrated in Fig.8 & Fig.9 bottom panels for the 3dKA and 3dHP models, respectively. The SEB temperature for different rods is the value of  $1/T$  at which  $y/y^* = 1.1$ . Here  $y(T, L) = D_{CM}\tau_\alpha^{1.25}$  and  $y^*(L) = y(2.0, L)$ . This procedure is very similar to the one adopted in Ref.[10]. The solid lines in these figure's bottom-center panel are the fit to function  $\ln(y/y^*) = [x + c_0(x/x_0)^n + c_1(x/x_0)^{2n}]$  where  $x = 1/T$ .

## IV. ROTATIONAL QUANTITIES

### A. Rotational correlation function

The  $l^{th}$  order rotational correlation function in three dimensions is defined as,

$$g_l(t) = \langle P_l(\cos[\theta(t)])P_l(\cos[\theta(0)]) \rangle \quad (14)$$

Where  $P_l$  is the  $l^{th}$  order Legendre Polynomial. In the single-molecule linear-dichroism experiments one get the major contribution to the auto-correlation function from  $g_2(t)$ , which in-turn is linked to the rotational diffusion constant as  $g_l(t) = \exp(-D_r l(l+1)t)$ . Also the non-exponential decay of these correlation function is the identification of dynamical heterogeneity in the system.

### B. Rotational Non-Normal Parameter

The rotation non-normal parameter (NNP),  $\alpha_{3D}^{rot}(t)$  is a function of fourth and second order moments for rotational motion combined in way to give zero for homogeneous diffusion. In other words in heterogeneous system, NNP would be a measure of fluctuation in the rotational diffusion constant at that time. For three dimensions following is the NNP [11]. Validity of the same can be checked by solving the rotational diffusion equation and finding the respective moments.

$$\alpha_{3D}(t) = \frac{1}{2} \frac{\langle |\hat{u}(t) - \hat{u}_0|^4 \rangle}{(\langle |\hat{u}(t) - \hat{u}_0|^2 \rangle)^2} + \frac{1}{6} \langle |\hat{u}(t) - \hat{u}_0|^2 \rangle - 1 \quad (15)$$

## V. STOKES-EINSTEIN-DEBYE RELATION

For rotational dynamics we have the Debye relation linking the rotational diffusion constant ( $D_r(T, L)$ ) with  $l^{th}$  order rotational correlation time  $\tau_l^r$  which is defined as the time when  $l^{th}$  order rotational correlation function  $g_l(t, T)$  (Eq:14) reduces

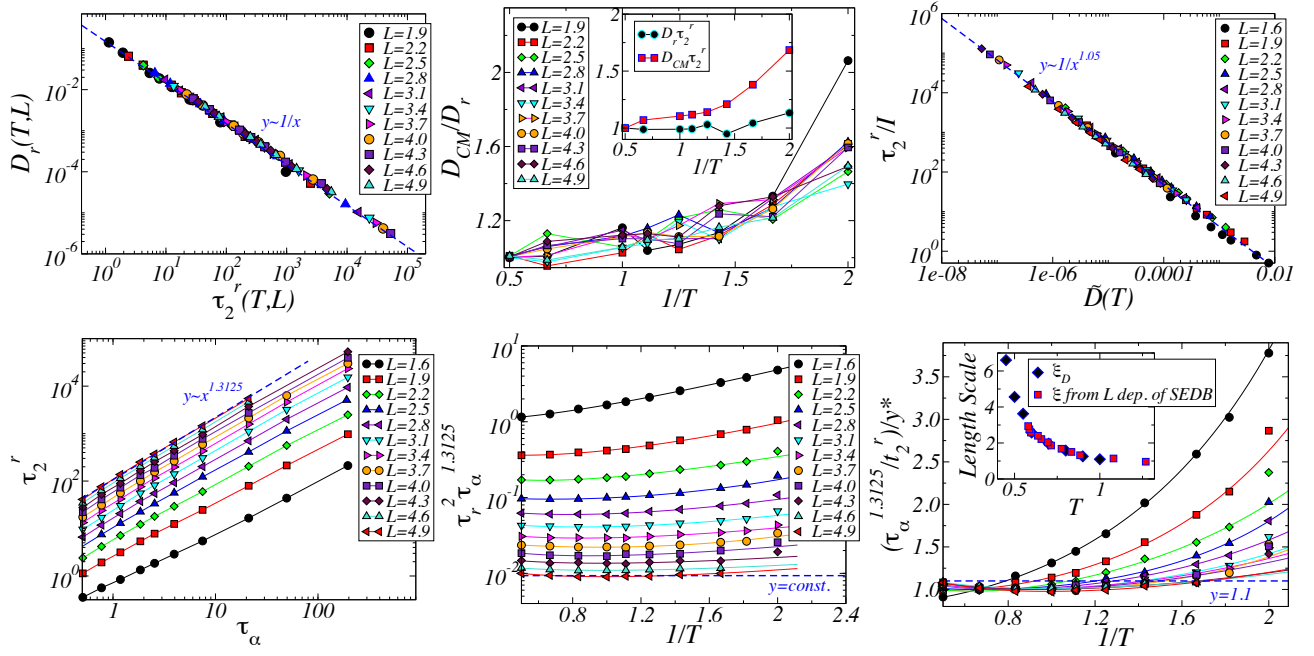


FIG. 10: In top-left panel the Debye relation for rotational diffusion constant and rotational relaxation time,  $D_r(T, L) \sim \frac{1}{\tau_2^r(T, L)}$  is tested in their cross plot for rods in 3dKA model system. In top-center panel, the ratio  $D_{CM}/D_r$  is plotted w.r.t. inverse temperature. According to SED relation this ratio should remain constant with temperature, thus its increase with decreasing temperature would lead to a conclusion of decoupling of translational-rotational dynamics of the probe rods. This supercooling effect of enhancement in the translational motion as compared to rotational motion is also inferred from  $D_r \tau_2^r$  and  $D_{CM} \tau_2^r$  plots for the rod of length  $L = 4.5$  in the inset. The cross plot of  $\tau_2^r/I$  and  $\tilde{D}(T, L)$  in the top-right panel predicts the power-law of  $\tau_2^r \sim D_{CM}^{-1.05}$ , which is again consistent with the enhancement of translation with supercooling. This direct link also enable us to perform the same SE-breakdown analysis on SED-breakdown to extract the dynamic length scale. The same for 3dKA system is highlighted in the bottom panels.

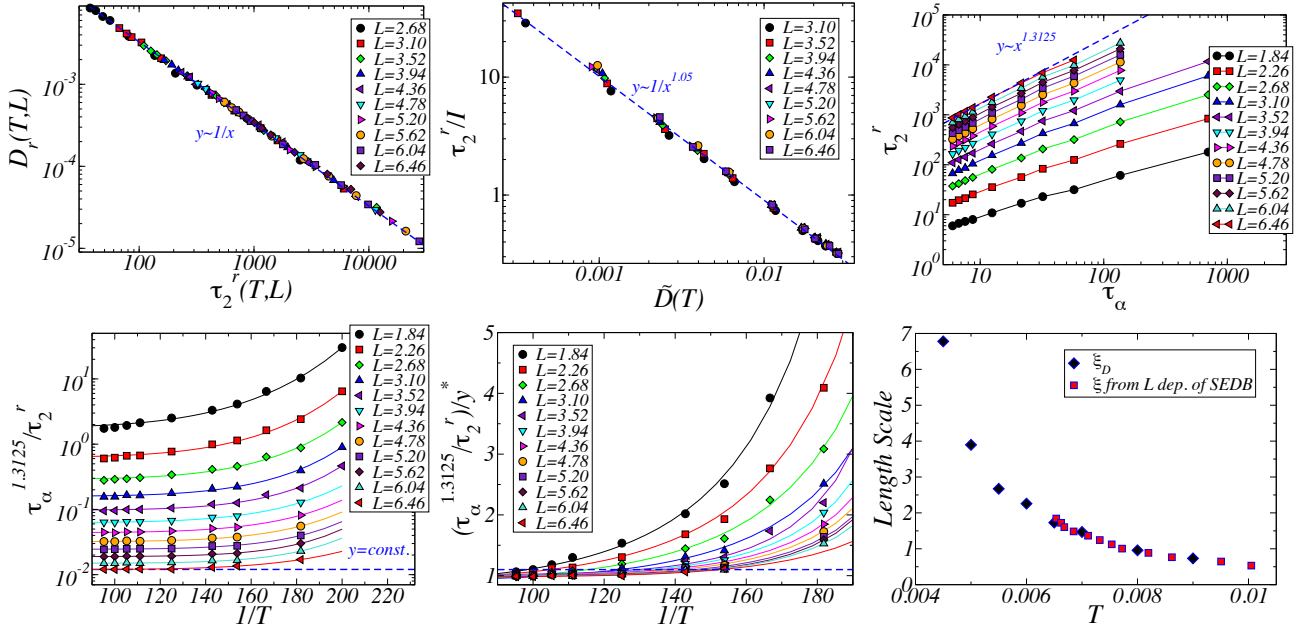


FIG. 11: Similar quantities are plotted as in Fig.10 for 3dHP model system.

to  $1/e$ . The Debye relation reads,  $D_r = 1/\tau_l^r l(l+1)$ , implying the factor  $D_r \tau_l^r$  is independent of temperature. In top-left panel of Fig.10 & Fig.11 this has been checked in the cross plot of  $D_r$  and  $\tau_2^r$  for various rod lengths in 3dKA & 3dHP model



respectively. The  $D_r \sim 1/\tau_2^r$  suggests that the Debye relation has survived the supercooled environment. Now if we combine the Debye relation with rotational SE relation i.e.  $D_r = k_B T / 8\pi\eta R^3$  then we would have the following Stokes-Einstein-Debye (SED) relation,

$$\frac{1}{\tau_r^l(l+1)} = \frac{k_B T}{8\pi\eta R^3} \quad (16)$$

and with the replacement of  $\eta$  with relaxation times, we have  $\frac{\tau_l^r}{\tau_{CM}^r}$  and  $\frac{\tau_l^l}{\tau_\alpha^l}$  as the SED parameters. Now as discussed in the main text, the translational motion gets decoupled from the rotational motion with supercooling. This phenomenon can be seen in Fig.10 (top-center) where ratio the  $D_{CM}/D_r$  grows with supercooling, regardless of the rod size. Also, the same can be verified from the cross plots of  $\tau_2^r$  and  $D_{CM}$  (top-right panel of Fig.10 & Fig.11). This implies that the self-SED relations are violated with increasing supercooling regardless of the probe size. From the observed power laws namely,  $\tau_2^r \sim D_{CM}^{-1.05}$  and  $D_{CM} \sim \tau_\alpha^{-1.25}$ , one expects  $\tau_2^r \sim \tau_\alpha^{1.3125}$  along with similar information of dynamic length scale contained in the rod-length dependence of the breakdown-temperature for this relation. The analysis for SED-Breakdown is presented in Fig.10 & Fig.11 for 3dKA and 3dHP model systems, along with the comparison of length scale obtained. The rotational relaxation time  $\tau_2^r(L, T)$  is easy to obtain experimentally than the translational quantities hence gives an advantage to the analysis.

## VI. EXISTING EXPERIMENTAL STUDIES

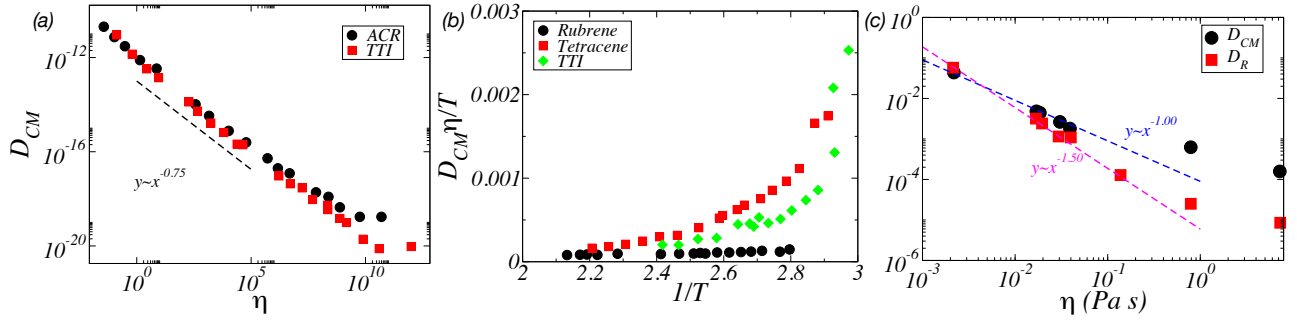


FIG. 12: (a) The  $D_{CM}$  of probes is plotted against the viscosity  $\eta$  of supercooled *OTP* [12]. One can clearly see the emerging power law and the deviation from it for different probes. The result is very similar to what we were expecting. (b) The SE parameter  $D_{CM}\eta/T$  is plotted for three different probes in supercooled *TNB* [13]. Again the results are in agreement of our simulation results. Note that hydrodynamic radius of *Rubrene* is larger than *TTI* while hydrodynamic radius of *Tetracene* is smaller than *TTI*. The breakdown temperature is then expected to be smallest the largest probe size i.e. *Rubrene*. We also highlight that this current experimental dataset is not enough to get a good estimate of the growing heterogeneity length scale but it certainly proves its existence. (c) The  $D_{CM}$  and  $D_R$  of tracer clusters are plotted against  $\eta$  of supercooled polymer fluid to highlight the different power-laws and deviation from it with increasing supercooling [14].

As mentioned in the main text, there are many single molecule experiments in literature which concentrate on the translation along with rotation of the probe molecule to quantify dynamic heterogeneity in supercooled liquids. The experiments reported mostly the variation of translational ( $D_{CM}$ ) and rotational ( $D_R$ ) diffusion constant with shear viscosity  $\eta(T)$ . Since  $\eta(T)$  for supercooled liquids is known to show diverging behaviour upon approaching the glass transition temperature,  $T_g$ , so the question usually addressed was, is  $D_{CM}$  &  $D_R$  also follows the  $T/\eta$  or they get decoupled? In Ref [12] the same was checked for various probes in *othoterphenyl (OTP)* and *salol*. It was found that  $D_{CM}$  have weaker temperature dependence of  $D_{CM} \sim \eta^{-0.75}$  for probes than the rotational diffusion constant,  $D_R \sim \eta^{-1}$  for self *OTP* particles. This result is shown in Fig.12 (a) for two different probes, *Aberchrome 540 (ACR)* and *2,2-bis(4,4-dimethylthiotan-3-one (TTI)* in supercooled *OTP*. One can very clearly see the effect of probe size in the deviation from this power-law, as proposed in our work. This experiment uses H-NMR stimulated echo method in static magnetic gradients. In another work by Blackburn et al.[13] the SE quantity  $D_{CM}\eta/T$  was calculated for various probes in supercooled *1,3,5-Tris(naphthyl)benzene (TNB)*. In Fig.12(b), one can clearly see the effect of probe size here as well in the SEB temperature. The probes used were *rubrene*, *tetracene* and *TTI*. Note that *rubrene* has larger hydrodynamic radius than *TTI* while *tetracene* has smaller hydrodynamic radius than *TTI*. Thus it is expected that *tetracene* will have SEB temperature that is much higher than either *TTI* or *rubrene*. This is in complete agreement with what is observed in our simulations. Thus it is clear that systematic experimental measurements on various probes with changing linear size will definitely lead to extraction of dynamic heterogeneity length scale in these molecular glass-forming liquids. We also want to highlight that this extracted data from existing experimental results are not good enough to extract the underlying length scale but it clearly demonstrate that our proposal is very robust and experimentally feasible. Lastly the deviation from the power laws

$D_{CM} \sim \eta^{-1.0}$  and  $D_R \sim \eta^{-1.50}$  with increasing supercooling can also be seen for tracer clusters in colloidal supercooled fluids in Fig.12 (c). This data is adapted from Ref.[14].

In the main text we illustrated a table containing various probes already been used in various supercooled liquids. The full description table with full chemical names is provided in the following table.

Medium	Probe
Glycerol	(a) <i>N,N'</i> -bis(2,5- <i>tert</i> -butylphenyl)-3,4,9,10-perylenedicarboximide ( <i>tbPDI</i> ) [15, 16] (b) <i>N,N'</i> -bis-(2,6-dimethylphenyl)-3,4,9,10-perylenedicarboximide ( <i>dpPDI</i> ) [15] (c) <i>N,N'</i> -bis[3-(dimethylamino)propyl]-3,4,9,10-perylenedicarboximide ( <i>dapPDI</i> ) [15] (d) <i>rubrene</i> molecule [17] (e) Gold nano-rods [18]
<i>ortho-terphenyl</i> (OTP)	(a) <i>rubrene</i> [19, 20] (b) 9,10-bis(phenylethynyl)anthracene ( <i>BPEA</i> ) [20] (c) <i>tetracene</i> [19–21] (d) <i>anthracene</i> [20, 21] (e) <i>dpPDI</i> (f) <i>tbPDI</i> (g) <i>N,N'</i> -bis(triethylglycol)-3,4,9,10-perylenedicarboximide ( <i>egPDI</i> ) (h) <i>N,N'</i> -dipentyl3,4,9,10-perylenedicarboximide ( <i>pPDI</i> ) [22] (i) <i>BODIPY268</i> dye [23]

## VII. MODEL SYSTEMS & SIMULATION DETAILS

**3dKA Model:** The 3dKA model is a generic model to mimics the molecular liquids ( $Ni_{80}P_{20}$  glass-forming liquids). It comprise of 80:20 binary mixture of A and B type Lennard-Jones particles. The interaction potential is given by

$$V_{\alpha\beta}(\mathbf{r}) = 4\epsilon_{\alpha\beta} \left[ \left( \frac{\sigma_{\alpha\beta}}{r} \right)^{12} - \left( \frac{\sigma_{\alpha\beta}}{r} \right)^6 \right] \quad (17)$$

where  $\alpha$  and  $\beta$  varies in A, B and the interaction strengths and radii are  $\epsilon_{AA} = 1.0$ ,  $\epsilon_{AB} = 1.5$ ,  $\epsilon_{BB} = 0.5$ ;  $\sigma_{AA} = 1.0$ ,  $\sigma_{BB} = 0.88$  and  $\sigma_{AB} = 0.8$ . The interaction is truncated at  $r = 2.5\sigma_{\alpha\beta}$  and is made smooth by adding upto 4<sup>th</sup> order terms. The simulations are done in temperature range  $T = 0.45, 1.00$  while the pressure is chosen to maintain the average number density  $\rho = 1.2$  with  $N = 5000$  particles.

**3dHP Model:** The 3dHP model is a paradigmatic model to study jamming physics in the context of dense, soft sphere systems and soft granular particles, including colloidal particles in experiments. It is a 50:50 binary mixture of harmonic spheres with diameter ratio 1.4 and interacting via potential,

$$V_{\alpha\beta}(\mathbf{r}) = \epsilon \left[ 1 - \left( \frac{r_{\alpha\beta}}{\sigma_{\alpha\beta}} \right) \right]^2 \quad (18)$$

for  $r_{\alpha\beta} < \sigma_{\alpha\beta}$  and  $V_{\alpha\beta} = 0$  otherwise, where  $\sigma_{\alpha\beta} = \frac{(\sigma_{\alpha} + \sigma_{\beta})}{2}$  and  $\epsilon = 1$ . Again as in 3dKA, its pressure is chosen to keep average number density,  $\rho = 0.82$  with  $N=5000$ , while the temperature is varied between  $\{T = 0.0050, 0.0090\}$

**Rods:** The embedded probe rods in the glass forming liquids are made of variable number of spheres,  $N_b$ , center of each sphere is separated from the consecutive sphere by a fixed distance of  $0.3\sigma_{AA}$  for 3dKA model and  $0.42\sigma_{AA}$  for 3dHP model. Each sphere of the rod have a same mass and interacts via same potential as any other sphere in the system. The interaction parameters are spheres in the rod are,  $\sigma_{RodSphere} = 1$ ,  $\epsilon_{RodSphere} = 1$ ,  $\sigma_{RodRod} = 1$  and  $\epsilon_{RodRod} = \frac{1}{2}$  same for all models. The rod length is defined as  $L = 0.3 * (N_b - 1) + 1.0$  for 3dKA and 2dmKA models and  $L = 0.42 * (N_b - 1) + 1.0$  for 3dHP model.

We have done NPT simulations for the models stated. Equation of motion for translational dynamics of spheres and center of mass (CoM) of rods is integrated by usual Leap-Frog integrator. The dynamics of rod's orientation vector ( $\hat{\mathbf{u}}$ ) is also integrated by the same integrator but strictly following the methods illustrated in [24, 25]. The temperature and pressure in the simulation is controlled by Berendsen thermostat and barostat [25]. A different thermostat does not change the results qualitatively. We reached this conclusion by checking our results with following different thermostat-barostat pairs, (a) three chain Nose-Hoover thermostat-barostat, (b) Gaussian thermostat Berendsen barostat, (c) Berendsen thermostat-barostat. For consistency between the schemes, we have used same time damping constants for both Berendsen and Nose-Hoover, viz  $\tau_T = 0.2$  and  $\tau_P = 2.0$  in reduced units. We have performed a consistency check on various quantities relevant to the results reported with above

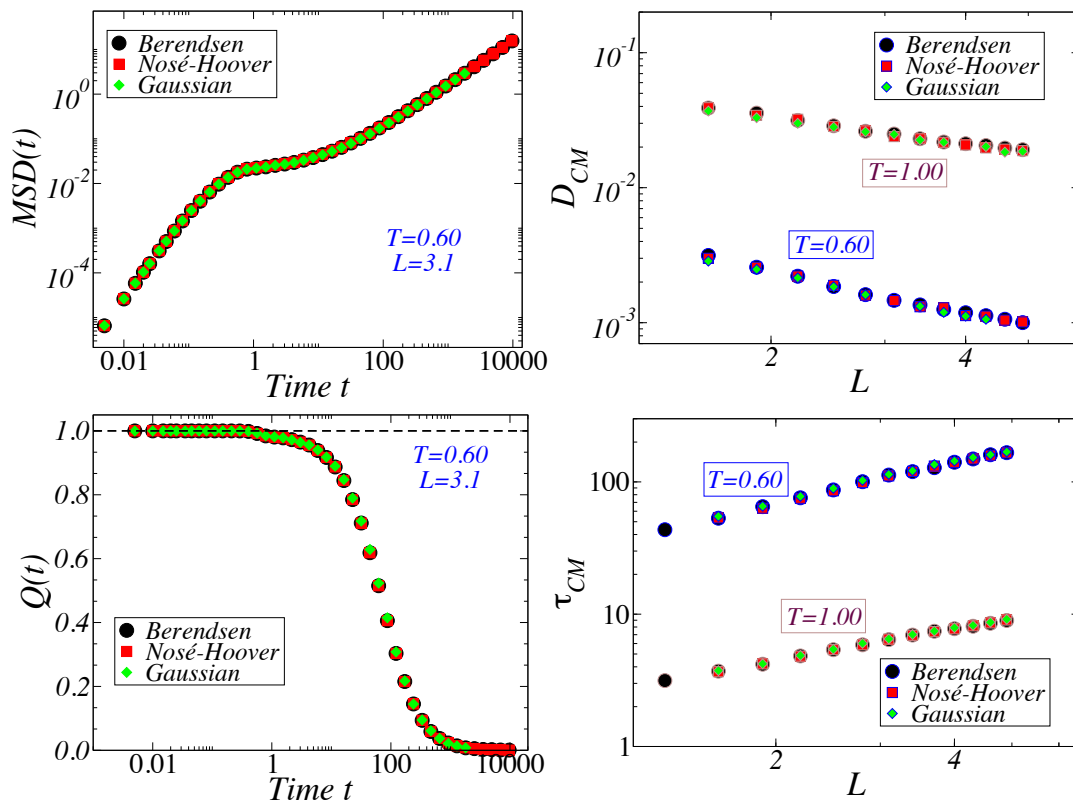


FIG. 13: The time evolution of MSD using various thermostat-barostat combinations is shown in the top-left panel. The plots are for length  $L = 3.1$  immersed in 3dKA model system at temperature,  $T = 0.60$ . Here *Berendsen* refers to Berendsen thermostat-barostat, *Nosé-Hoover* refers to three-chain Nosé-Hoover thermostat-barostat, and *Gaussian* refers to Gaussian thermostat-Berendsen barostat. The rod length variation of diffusion constant obtained from the MSD's is plotted in the top-right panel for two different temperatures, namely  $T = 0.60$  and  $T = 1.00$ . In the very similar way the overlap-correlation function,  $Q(t)$  and the relaxation time and  $\tau_{CM}(T, L)$  is plotted in the bottom panel. The equivalence in all of these quantities with different thermostat-barostat suggests the independence of the reported results on thermostats and barostats.

mentioned thermostat-barostat schemes, and is shown in Fig.13. More details about the various thermostats and barostats can be found in Ref.[25].

- 
- [1] C. Dasgupta, A. V. Indrani, S. Ramaswamy, and M. K. Phani, *Europhysics Letters* **15**, 307 (1991), URL <https://doi.org/10.1209/0295-5075/15/3/013>.
  - [2] L. Berthier, G. Biroli, J.-P. Bouchaud, L. Cipelletti, and W. van Saarloos, eds., *Dynamical Heterogeneities in Glasses, Colloids, and Granular Media* (Oxford University Press, 2011), URL <https://doi.org/10.1093/acprof:oso/9780199691470.001.0001>.
  - [3] G. Biroli, J.-P. Bouchaud, A. Cavagna, T. S. Grigera, and P. Verrocchio, *Nature Physics* **4**, 771 (2008), ISSN 1745-2481, URL <https://doi.org/10.1038/nphys1050>.
  - [4] S. Karmakar, C. Dasgupta, and S. Sastry, *Proceedings of the National Academy of Sciences* **106**, 3675 (2009), ISSN 0027-8424, <https://www.pnas.org/content/106/10/3675.full.pdf>, URL <https://www.pnas.org/content/106/10/3675>.
  - [5] S. Karmakar, E. Lerner, and I. Procaccia, *Physica A: Statistical Mechanics and its Applications* **391**, 1001 (2012), URL <https://doi.org/10.1016/j.physa.2011.11.020>.
  - [6] M. Doi and S. F. Edwards, *The theory of polymer dynamics*, no. 73 in International series of monographs on physics (Clarendon Press, Oxford, 2007), reprinted ed., ISBN 9780198520337, oCLC: 845169495.
  - [7] A. Mutneja and S. Karmakar, *Dynamics of rod like particles in supercooled liquids – probing dynamic heterogeneity and amorphous order* (2020), 2005.11063.
  - [8] L. D. Landau, *Fluid Mechanics: Landau and Lifshitz: Course of Theoretical Physics, Volume 6* (Pergamon, 2013), URL <https://www.xarg.org/ref/a/B00JO9YOS2/>.
  - [9] Z. Shi, P. G. Debenedetti, and F. H. Stillinger, *The Journal of Chemical Physics* **138**, 12A526 (2013), URL <https://doi.org/10.1063/1.4800000>.

1063/1.4775741.

- [10] A. D. Parmar, S. Sengupta, and S. Sastry, *Physical Review Letters* **119** (2017), URL <https://doi.org/10.1103/physrevlett.119.056001>.
- [11] R. Jain and K. L. Sebastian, *The Journal of Chemical Physics* **146**, 214102 (2017), URL <https://doi.org/10.1063/1.4984085>.
- [12] I. Chang, F. Fujara, B. Geil, G. Heuberger, T. Mangel, and H. Sillescu, *Journal of Non-Crystalline Solids* **172**, 248 (1994), ISSN 0022-3093.
- [13] F. R. Blackburn, C.-Y. Wang, and M. D. Ediger, *The Journal of Physical Chemistry* **100**, 18249 (1996), ISSN 0022-3654.
- [14] K. V. Edmond, M. T. Elsesser, G. L. Hunter, D. J. Pine, and E. R. Weeks, *Proceedings of the National Academy of Sciences* **109**, 17891 (2012), ISSN 0027-8424.
- [15] S. A. Mackowiak, L. M. Leone, and L. J. Kaufman, *Phys. Chem. Chem. Phys.* **13**, 1786 (2011), URL <https://doi.org/10.1039/c0cp01860k>.
- [16] R. Zondervan, F. Kulzer, G. C. G. Berkhout, and M. Orrit, *Proceedings of the National Academy of Sciences* **104**, 12628 (2007), URL <https://doi.org/10.1073/pnas.0610521104>.
- [17] S. A. Mackowiak, T. K. Herman, and L. J. Kaufman, *The Journal of Chemical Physics* **131**, 244513 (2009), URL <https://doi.org/10.1063/1.3277141>.
- [18] H. Yuan, S. Khatua, P. Zijlstra, and M. Orrit, *Faraday Discussions* **167**, 515 (2013), URL <https://doi.org/10.1039/c3fd00091e>.
- [19] M. T. Cicerone and M. D. Ediger, *The Journal of Chemical Physics* **103**, 5684 (1995), URL <https://doi.org/10.1063/1.470551>.
- [20] M. T. Cicerone and M. D. Ediger, *The Journal of Chemical Physics* **104**, 7210 (1996), URL <https://doi.org/10.1063/1.471433>.
- [21] M. T. Cicerone and M. D. Ediger, *The Journal of Physical Chemistry* **97**, 10489 (1993), URL <https://doi.org/10.1021/j100142a037>.
- [22] L. M. Leone and L. J. Kaufman, *The Journal of Chemical Physics* **138**, 12A524 (2013), URL <https://doi.org/10.1063/1.4773889>.
- [23] K. Paeng, H. Park, D. T. Hoang, and L. J. Kaufman, *Proceedings of the National Academy of Sciences* **112**, 4952 (2015), URL <https://doi.org/10.1073/pnas.1424636112>.
- [24] D. C. Rapaport, *The Art of Molecular Dynamics Simulation* (Cambridge University Press, 2004), 2nd ed.
- [25] M. P. Allen and D. J. Tildesley, *Computer Simulation of Liquids* (Clarendon Press, New York, NY, USA, 1989), ISBN 0-19-855645-4.